Contribution to XXIV International Cosmic Ray Conference (Aug. 28 – Sep. 8, 1995, Rome) from Chacaltaya and Pamir Emulsion Chamber Experiments †

Chacaltaya and Pamir Collaborations
(edited by A. Ohsawa)

† The experiments are financially supported in part by Institute for Cosmic Ray Research, University of Tokyo.

Content

I. Highlight Session "Very High Energy Cosmic Ray Interactions (Super-families)"

(1) "Attenuation Mean Free Path of Hadrons in Super-Families" 1
(2) "Simultaneous Observation of Families and Associated Air Showers at Mt. Chacaltaya" 7
(3) "Preliminary Report on the Large Halo Event TADJIKISTAN" 13

II. Sessions.

(1) "Comments to Short Mean Free Path Particles Observed by Pamir Thick Lead Chambers" 19
(2) "Nuclear Interaction Families Associated to EAS at Mt. Chacaltaya" 23
(3) "Violation of the Feynman Scaling Law in the Forward Region" 27
(4) "A Study of Shower Transition Behaviours Initiated by Hadron-Pb Interaction" 31
(5) "Attenuation Mean Free Path of High Energy Hadrons in Lead" 35
(6) "Wavelet Analysis of High Multiplicity Events" 39
(7) "'γ-rays' bundles at the cores of extensive air showers and the primary cosmic ray identification" 43
(8) "Production of Heavier Particles Than Pions in Fire-Balls" 47
(9) "Fire-Ball Masses Seen in C-jets" 51
(10) "A Double-core Events Detected at Chacaltaya" 54
(11) "Analysis of the Particle Production in Cosmic Ray Events Detected at Mt. Chacaltaya" 57
(12) "Nucleon-Air Nuclei Interaction Probability Law and the Inelastic Cross-Section" 61

Attenuation Mean Free Path of Hadrons in Super-Families.

Vladimir Kopenkin and Yoichi Fujimoto
Institute for Nuclear Physics, Moscow State University,
Adv. Res. Center for Science and Technology, Waseda University.

1. Introduction.

As was reported at the previous conference (ref 1), the result of experiment with thick Pb-chambers of Pamir gave an unexpectedly small value for the attenuation mean free path for hadrons in super-families. It is 170 +47 -26 g/cm^2 in Pb with 95% CL by maximum likelyhood method. This is to be compared with the value for hadrons of single arrival, 200 - 250 g/cm^2, which was repeatedly measured by Moscow University group (ref 2).

The result was obtained from a number of thick Pb-chambers of Moscow University type, and the observation was for hadrons with energy > 10 TeV. The super-families observed here are 17 events with energy-sum > 700 TeV, while the majorities are with energy of 2,000 - 3,000 TeV.

Comparing with the geometrical collision mean free path, about 192 g/cm^2 in Pb, the above value is unexpectedly short, and the authors suggested its possible connection to interactions of the exotic-type proposed by Chacaltaya Collaboration (ref 1, and 3).

Because of importance of the results, we made a systematic study with four chambers of recent exposure at Pamir for the check, and the present report gives the preliminary results. The four chambers are all with the same structure of thick Pb type, and the measurement was made by a joint team of Waseda and Moscow University all through the work. The study covers all showers above the detection threshold, both of single arrival as well as in a family. The simulation calculation was made by Tamada (ref 3), and the comparison was made in every steps of the analysis.

2. Outline of the present experiment.

The four chambers of the present experiment are all with thickness of 60 cm of Pb, and the X-ray film (RT6M, Russian-made) are placed at every 1 cm of Pb throughout the chamber except at the very top.

Attenuation m.f.p. of hadrons with E > 10 TeV

category of hadrons	number of hadron shower	attenuation m.f.p. in Pb (g/cm^2)
single arrival	911	214 ± 14
in family (E > 100 TeV)	141	233 ± 40

The hadron attenuation mean free path is a function of the collision mean free path, inelasticity of the collision K , and power of the energy spectrum of a hadron. With the observed value of the power, we arrive at the following conclusion (for detailed discussion, see Tamada (ref 4);

i) The hadrons of single arrival as well as of families are with the collision cross section with Pb, close to the geometrical size of Pb-nucleus and the average inelasticity 0.7 - 0.8.

ii) The short mean free path of hadrons is observed only in super-families beyond energy of 1,000 TeV, but not in families with several hundred TeV.

4. Hadrons and gamma-rays in family.

This type of thick Pb chamber is good for hadron detection, with detection efficiency close to 1. It gives a chance to make complete observation of hadron-gamma families, which is not possible with other types of chambers. Here, we show in Fig. 3 the N_h-Q_h diagram for the observed families together with the simulation results, as an example. N_h expresses number of hadrons and Q_h the ratio of hadron energy sum over the total energy in a family.

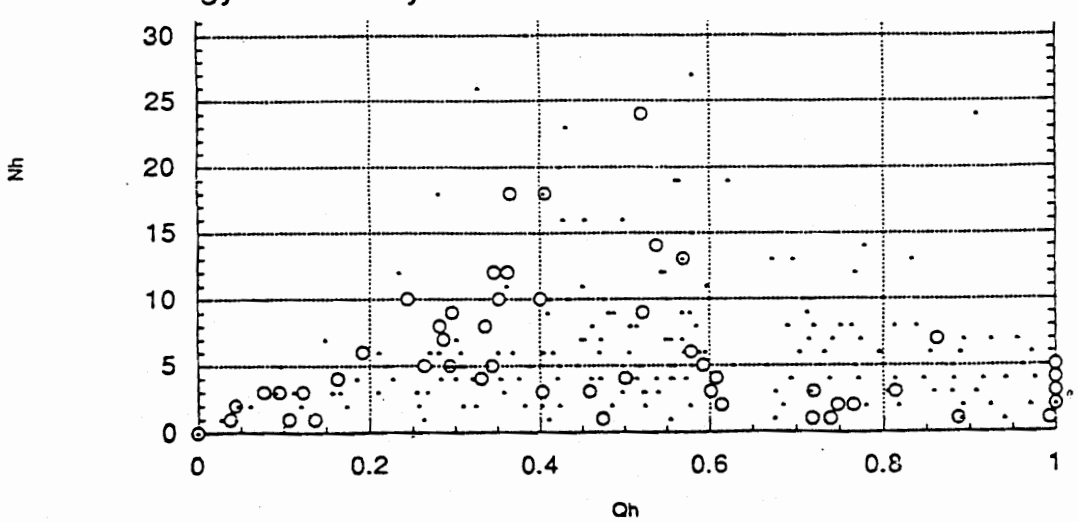

Fig.3 Nh-Qh diagram, circles for experiment and dots for simulation.

Seeing Fig. 3 of the diagram, one finds that the points showing observed families in the experiment distribute over the same region of the diagram as those obtained by the simulation calculation. There is found no evidence, within the limit of statistics, of a cluster of points showing a particular hadron-rich type of exotic events (ref 3). Thus, events of those exotic types exist with frequency less than the previously estimated value, may-be appreciable only in super-family region.

The following diagram of Q_h, in Fig 4, gives an example of comparison with simulation results. Here one sees a uniform distribution of Q_h in the experiment, while the simulation shows a peak at Q_h around 0.5 . A simple explanation can be that the charge state of individual emitted pions is not just at random as in the assumed case for simulation.

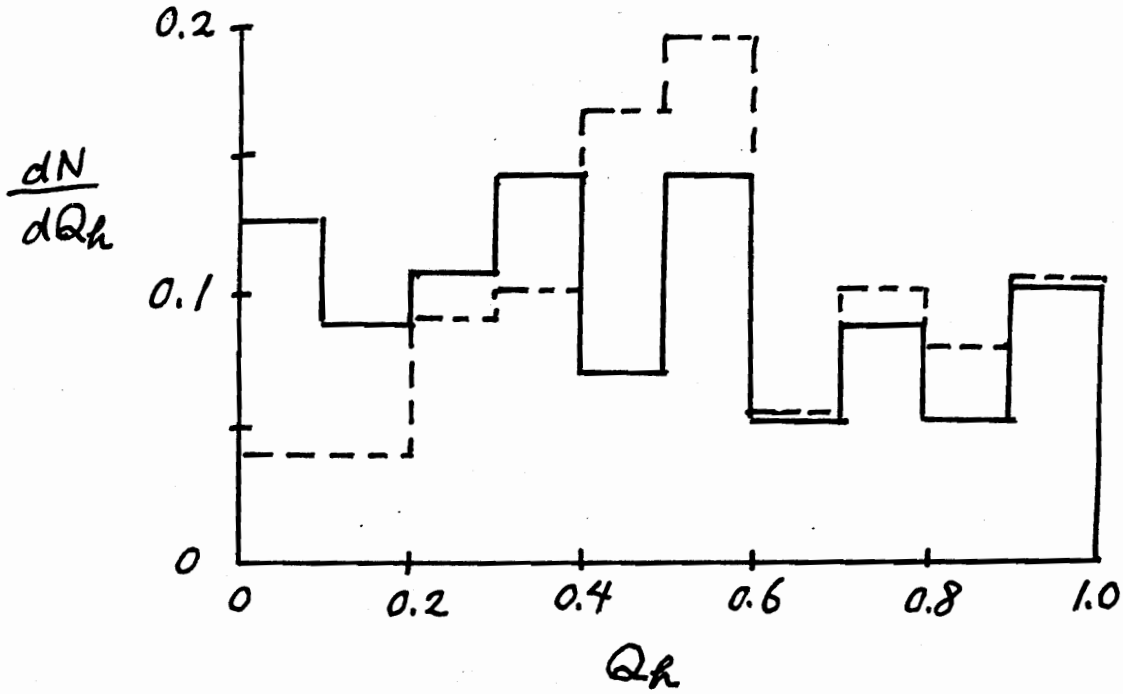

Fig.4 Normalized Q_h-distribution, a solid line for experiment and a broken line for simulation.

5. Preliminary results of family analysis.

The family analysis is made through the following steps;

1) decascading through making cluster of gamma-rays with constant K_{decas} = 12 TeVmm, for picking up an air cascade.

2) jet-clustering through making cluster of decascaded gamma-rays and hadrons with constant K_{jet} = 200 TeVmm, for picking up a jet produced in the nuclear cascade.

3) rejuvenation by setting the threshold, f_{min} = 0.04, for the fractional energy of a jet. This allows to normalize the data in energy scale, leaving a skelton of the nuclear cascade.

The comparison with the simulation data is made in every steps, and we found agreement within the statistical error. It shows that the nuclear interaction follows approximately along the extrapolation of the collider information. The obtained full results will be presented in a publication elsewhere.

References

1) T.Arisawa et.al.(Chacaltaya and Pamir Collaboration), Proc 23rd Int Cosmic-Ray Conf, Calgary(1993), vol 4, 136, and Nucl. Phys. B424 (1994), 241.

2) Pamir Collaboration, Bulletin de la societe des sciences et des lettres de Lodz, v.XII N 111-120 (1992), 119.

Pamir Collaboration, Proc Int Symp on Cosmic-Rays and Particle Phys, Tokyo(1984), 426.

I.P.Ivanenko et al, Proc Int Workshop on Super-High Energy Hadron Interactions, Tokyo(1991), 197 and 215.

Pamir Collaboration, Izvestija AN SSSR, 55(1991),650.

3) S.Hasegawa, AIP Conf Proc, No. 85(1980), 500.

Chacaltaya and Pamir Collaboration, Nucl. Phys. B370(1992), 365 and Proc 23rd Int Cosmic-Ray Conf, Calgary(1993), vol 4, 116, 120 and 124.

4) M.Tamada, J.Phys. G21(1995),1387.

Simultaneous Observation of Families and Associated Air Showers at Mt. Chacaltaya

N. Kawasumi, I. Tsushima, K. Honda, K, Hashimoto, T. Matano [1],
N. Inoue [2], K. Mori [2], K. Yokoi [3], A. Ohsawa [4], M. Tamada [5], N. Ohmori [6],
N. Martinic [7], R. Ticona [7], N. Gironda [7] F. Osco [7] and C. Aguirre [7]

Department of Physics, Yamanashi University, Kofu 400, Japan.
[1] *Dep. of Applied Phys. and Chem., Fukui Inst. of Technology, Fukui 910, Japan.*
[2] *Department of Physics, Saitama University, Urawa 338, Japan.*
[3] *Fac. of Sci. and Eng., Aoyama Gakuin University, Setagaya, Tokyo 157, Japan.*
[4] *Inst. for Cosmic Ray Research, University of Tokyo, Tanashi, Tokyo 188, Japan.*
[5] *Fac. of Science and Technology, Kinki University, Kowakae, Osaka 577, Japan.*
[6] *Department of Physics, Kochi University, Kochi 780, Japan.*
[7] *Inst. de Inv. Fisicas, Universidad Mayor de San Andres, La Paz, Bolivia.*

The observation of families and air showers is carried out at Mt. Chacaltaya (5,200 m, 540 g/cm^2 atmospheric depth, Bolivia), by operating the emulsion chamber and the air shower array simultaneously. We will summarize in this paper the results by the experiment, leaving the description of experimental apparatus, experimental procedure, etc. elsewhere.[1),2)] The analysis relies on the data of 47 families of $\Sigma E_\gamma \geq 10$ TeV with the accompaniment of air showers.

(i) Energy spectrum of γ-rays per family.

Energy spectra of γ-rays per family, in the experiment and in the simulation†, are shown in Fig. 1 for three different regions of air shower size $N_e = 10^5 \sim 10^6$, $10^6 \sim 10^7$ and $10^7 \sim 10^8$. The experimental data show that the spectra of different N_e regions differ in the number of γ-rays per family. Comparison of the spectra in the experiment and in the simulation shows that there is a discrepancy in the number of γ-rays, i.e. the experiment gives smaller number than the simulation, while the slopes of the spectra agree with each other.

HADRON, the same type of experiment at Tien Shan (3,300 m, 700 g/cm^2, Kazakhstan), reported that the spectrum, expressed by the variable $x = E_\gamma/E_0$ where E_0 is estimated from N_e by assuming $E_0/N_e = 2.0$ GeV, becomes steeper suddenly in the region $N_e > 10^7$, compared with those in lower size region.[5)] And they argue that

†UA5 simulation algorithm [3)] is employed for hadron-air collisions in the present simulation of high energy cosmic-ray phenomena in the atmosphere. It reproduces the features of multiple particle production at $\sqrt{s} = 200$, 546 and 900 (GeV), which shows a fair violation of Feynman scaling law in the forward region.[4)]

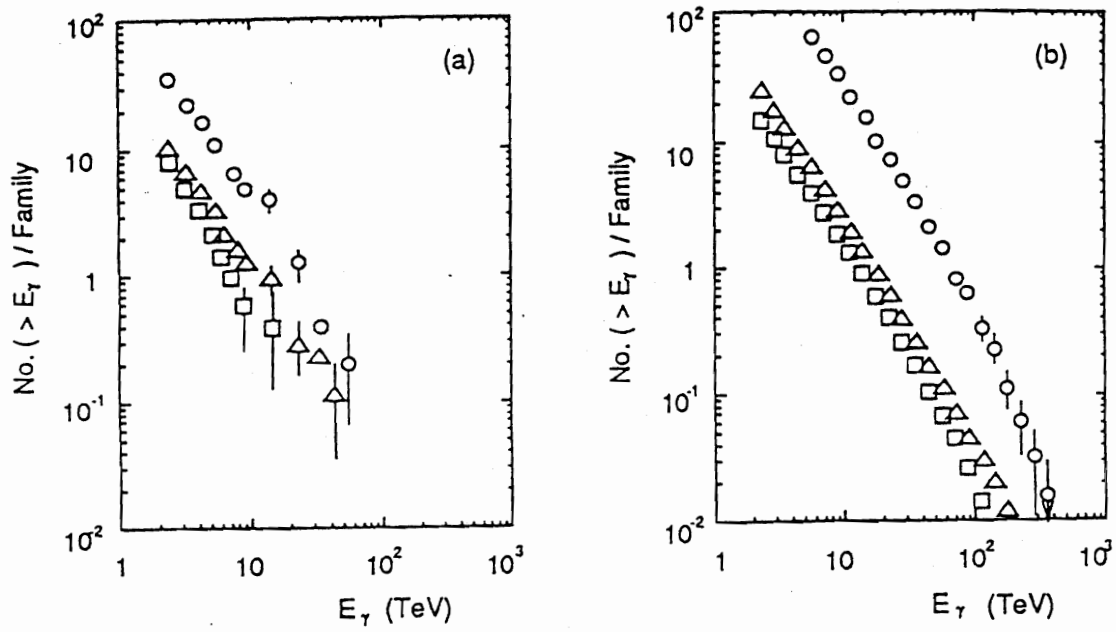

Fig. 1 Energy spectrum of γ-rays in the family for three regions of the size of the accompanying air showers ; $N_e = 10^5 \sim 10^6$ (□), $N_e = 10^6 \sim 10^7$ (△), and $N_e = 10^7 \sim 10^8$ (○). (a) experimental data and (b) simulation.

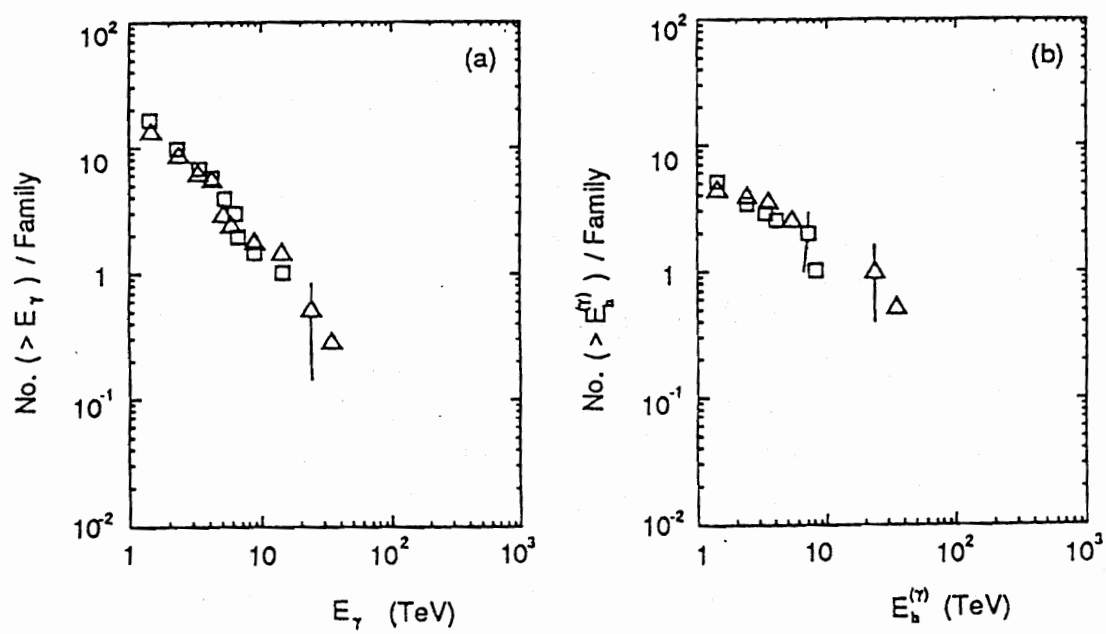

Fig. 2 Energy spectrum of γ-rays (a) and hadrons (b) per family for two groups of families. $E_h^{(\gamma)}$ in the figure (b) is the visible energy of the hadron-induced shower.
□ : Families with $\Sigma E_\gamma = 46.4 \sim 100$ (TeV) and $N_e = 10^5 \sim 10^6$,
△ : Families with $\Sigma E_\gamma = 46.4 \sim 100$ (TeV) and $N_e = 10^6 \sim 10^7$.

nuclear interaction changes its feature above $\sim 2 \times 10^{16}$ eV. However such a change of the slope is not observed in Fig. 1 by our experiment.

In order to study the relation between the families and the accompanied air showers in more detail, we compare the energy spectra of γ-rays per family, grouping the

events both by ΣE_γ and N_e. That is, all the families with $\Sigma E_\gamma = 10 \sim 215$ (TeV) are classified into four groups of $\Sigma E_\gamma = 10 \sim 21.5$, $21.5 \sim 46.4$, $46.4 \sim 100$ and $100 \sim 215$ (TeV). Fig. 2(a) shows the energy spectrum of γ-rays per family, for two groups of events with the same interval of $\Sigma E_\gamma = 46.4 \sim 100$ (TeV) and with different intervals of $N_e = 10^5 \sim 10^6$ and $10^6 \sim 10^7$, as an example. As can be seen in the figure, the energy spectra of the same interval of ΣE_γ agree well with each other in spite of the difference of size region. In other words, the energy spectrum of γ-rays in one family does depend on ΣE_γ of the family, but does not on N_e of the accompanied air shower. It is the case for the hadrons in the family, too. (See Fig. 2(b).)

It indicates that the family is produced deep in the atmosphere by a small number (one or two) interactions of high energy hadrons in the air shower. Therefore there is no sharp correlation between the characteristics of the family and those of the accompanied air shower.

Fig. 3 presents the energy spectra of γ-rays per family for four intervals of ΣE_γ, without classifying the events by N_e to improve the statistics. On the whole the spectra in the experiment and in the simulation agree with each other with respect to both the slope and the number of γ-rays.

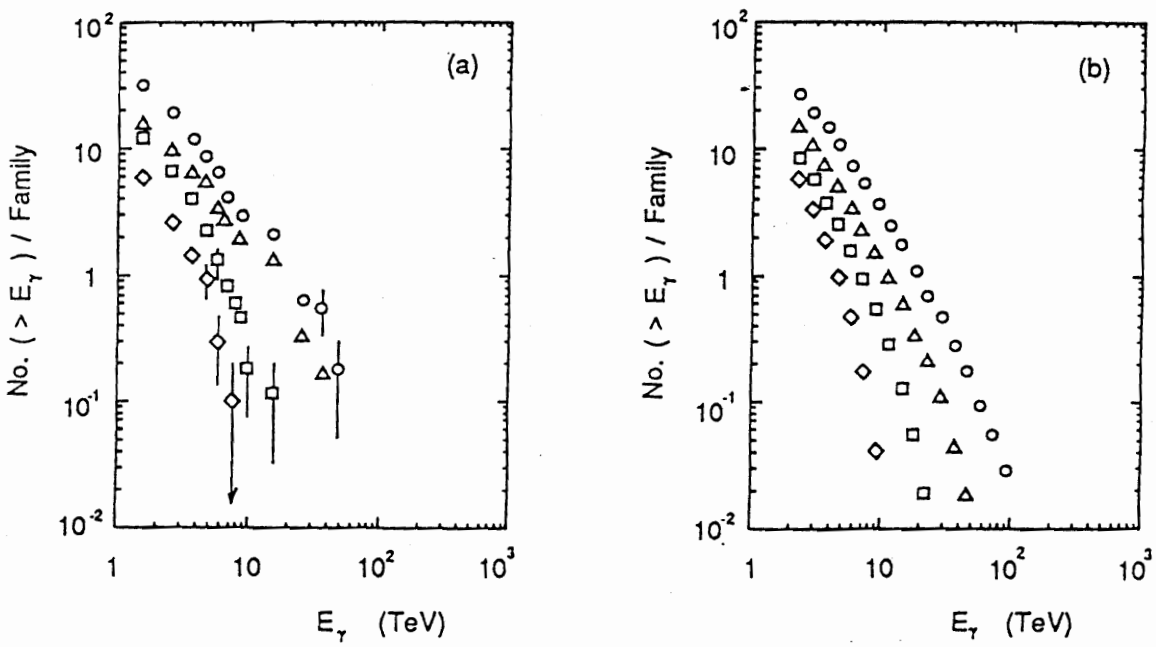

Fig. 3 Energy spectrum of γ-rays in the family for four regions of ΣE_γ, without classifying the data by N_e of the accompanying air shower. Figures (a) and (b) are by the experimental data and by the simulation.

$\diamond$: $10 \leq \Sigma E_\gamma$ (TeV) < 21.5, $\square$: $21.5 \leq \Sigma E_\gamma$ (TeV) < 46.4,
$\triangle$: $46.4 \leq \Sigma E_\gamma$ (TeV) < 100, $\circ$: $100 \leq \Sigma E_\gamma$ (TeV) < 215.

What are mentioned above for the γ-rays are valid for hadrons in the family, too.

To conclude the present subsection, our simulation code does simulate the features *inside* the family well, but does not the relation between the family and the air shower

(or between the family and the primary energy of the event).

(ii) Correlation between $< \Sigma E_\gamma >$ and N_e.

Fig. 4 presents the scatter diagram between ΣE_γ and N_e, and Fig. 5 the dependence of the average value of ΣE_γ on N_e in the experiment and in the simulation. In the simulation the center of the family is distributed randomly over one block of the emulsion chamber in order to take into account missing showers which fall outside the emulsion chamber, though the effect is found small.

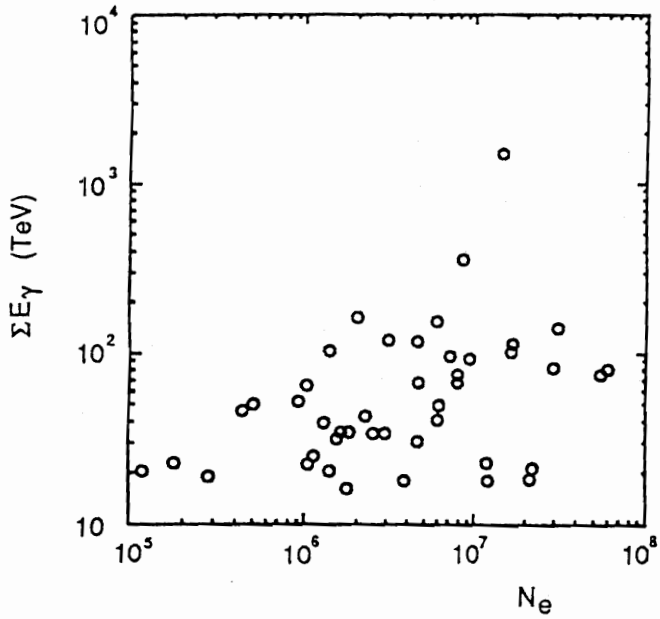

Fig. 4 Diagram between ΣE_γ (the total observed energy in the family) and N_e (the size of the air shower).

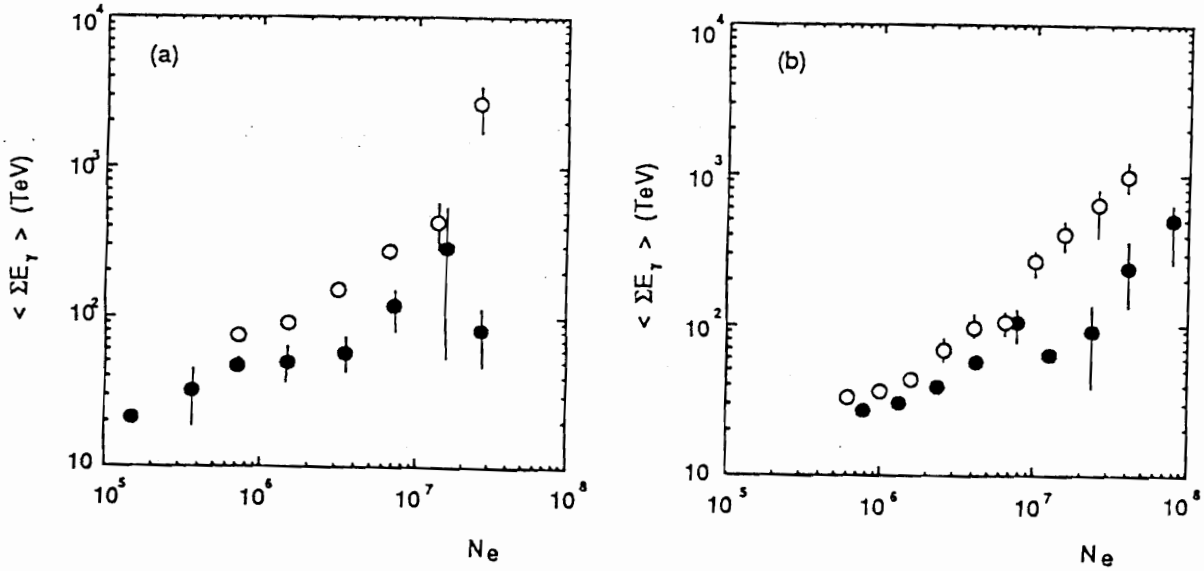

Fig. 5 Correlation between $< \Sigma E_\gamma >$ (the average value of ΣE_γ) and N_e. Figures (a) and (b) are by the present experiment and by HADRON experiment.[5] The full circles are by the experiment and the open circles by the simulation.

It is seen in Fig. 5(a) that $< \Sigma E_\gamma >$ of the experiment has a smaller value than that of the simulation. Similar tendency is seen by HADRON at Tien Shan,[5]. (Fig. 5(b)).

The discrepancy between the experiment and the simulation is found again in the relation between the family and the accompanied air shower.

The observed discrepancy, in Fig. 1 and in Fig. 5, indicates a more rapid energy dissipating process in the atmospheric propagation of cosmic rays at high energies. And the hypotheses for such a process under discussion are an increase of heavy components in the primary cosmic rays and the change of the nuclear interactions. The simulation shows, however, that the increase of iron component reduces the observed discrepancy only in part, because even iron primaries produce large families, whose $< \Sigma E_\gamma >$ is greater than the value of the experiment, in high energy region $N_e > 10^7$.[6] Hence the change of nuclear interaction is necessary for the required rapid energy dissipating process, whether one assumes the increase of heavy primaries or not.

It may be worthwhile to note the following points regarding the above analysis.
(1) The analysis is free from the absolute intensity of the primary cosmic-ray spectrum. It is the advantage of the present experiment, compared with the *pure* emulsion chamber or air shower experiment.
(2) It is not the reason for the ineffectiveness of the iron component to $< \Sigma E_\gamma >$ that most of the families, produced by the iron component, disappear in the atmosphere before arriving at the chamber, because the primary cosmic rays produce always the visible families in the region $N_e > 10^7$.
(3) For all of the 47 families with accompanying air showers, the family centers always coincide with the core position of air showers within the experimental error. Hence there is no possibility that the families are produced locally at the periphery of the large air showers.

Figs. 5(a) and (b) show that the experimental values of $< \Sigma E_\gamma >$, at Mt. Chacaltaya and at Tien Shan, are similar in spite of the difference of altitudes, while the simulation shows that $< \Sigma E_\gamma >$ at Mt. Chacaltaya is $2 \sim 3$ times as large as that at Tien Shan. The reason for it may be attributed to the fact that the energies of γ-rays are over-estimated in HADRON experiment, because ΣE_γ spectrum at Tien Shan is not consistent with those at Mt. Chacaltaya and at Mt. Fuji.

(iii) It is important to see what kind of families are produced by the air showers of a fixed size, or, more specifically, the distribution of ΣE_γ at a fixed value of N_e,

$$\varphi(x, N_e)\, dx \qquad \text{with} \qquad x = \Sigma E_\gamma \quad .$$

It can be observed in Fig. 4 directly along a fixed value of N_e, if the statistics of the events is large enough and if the most part of the distribution exists above the threshold of ΣE_γ. However unfortunately our experiment fulfills neither of the conditions. Hence we will discuss it in another way.

The distribution can be expressed approximately by a single variable of $\Sigma E_\gamma / {N_e}^\delta$, because we have $\Sigma E_\gamma \propto {E_0}^\delta$ approximately. That is,

$$\varphi(x, N_e)\, dx = \phi(\frac{x}{{N_e}^\delta})\frac{dx}{{N_e}^\delta} \quad .$$

The exponent $\delta = 1.44$ assures the difference of the exponent between ΣE_γ spectrum ($\beta = 1.25$) and N_e spectrum ($\gamma = 1.8$), because we have $\beta = \gamma/\delta$.

The distribution of $\Sigma E_\gamma / {N_e}^\delta$ by the experimental data is proportional to

$$\phi(y)\, dy \qquad \text{with} \qquad y = \frac{\Sigma E_\gamma}{{N_e}^\delta} \quad .$$

It means seeing the distribution of the events in Fig. 4 by rotating the y-axis from the vertical line to the slant line of $\Sigma E_\gamma \propto {N_e}^\delta$.

The distributions of the experiment (Fig. 6(b)) are broad compared with those of the simulation (Fig. 6(c)) where the events of proton primaries are sampled. It shows that the families are produced not only by protons (with UA5 algorithm of nuclear interactions in the atmosphere) but also by other processes. For example, the families produced by iron primaries contribute to the left-hand side part of the distribution.

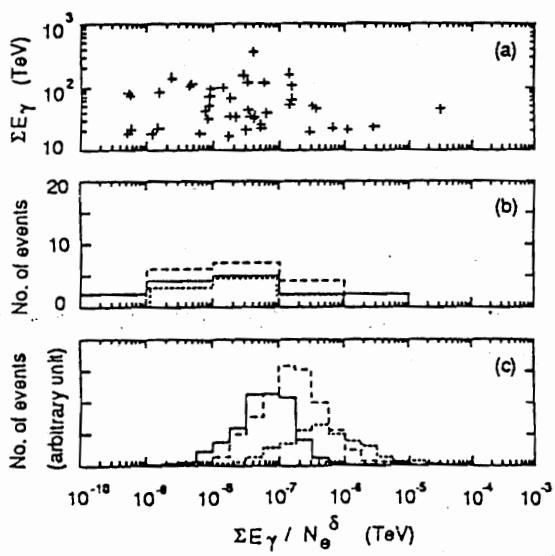

Fig.6 The distribution of $y = \Sigma E_\gamma / {N_e}^\delta$.
(a) Scatter plot of ΣE_γ of the families and $y = \Sigma E_\gamma / {N_e}^\delta$ where N_e is the size of the air shower. ΣE_γ is proportional to ${N_e}^\delta$ approximately. (See the text.)
(b) Histograms of $y = \Sigma E_\gamma / {N_e}^\delta$ for the events with a certain values of ΣE_γ, by the experiment.
solid line : $10 \leq \Sigma E_\gamma$ (TeV) < 31.6
dashed line : $31.6 \leq \Sigma E_\gamma$ (TeV) < 100
dotted line : $100 \leq \Sigma E_\gamma$ (TeV)
(c) The same as (b) by the simulation of proton primaries. The total area under the histograms is normalized to the histogram in (b).

References.

1) N. Kawasumi et al., AIP Conf. Proc. No.276 (1992) 88.
2) N. Kawasumi et al., Proc. 24th ICRC (Rome) Vol.1 (1995) 201
3) G.L. Alner et al. (UA5 Collaboration), Nucl. Phys. **B291** (1987) 445.
4) A. Ohsawa, Prog. Theor. Phys. **92** (1994) 1005.
5) V.V. Arabkin et al., FIAN Preprint No.140 (1991) (Lebedev Phys. Inst.)(in Russia), and Proc. 22nd ICRC (Dublin) Vol.4 (1991) 269 and 273.
6) M. Tamada, J. Phys. **G20** (1994) 487.

Preliminary Report on the Large Halo Event TADJIKISTAN

Akinori Ohsawa
Institute for Cosmic Ray Research, University of Tokyo,
Tanashi, Tokyo, 188 Japan.

I. Introduction.

A large event with a halo, called TADJIKISTAN, was observed by the emulsion chamber which was constructed at Pamirs by the collaboration of the former USSR countries and Poland. (Fig. 1) It consists of a halo (diameter $\sim$ 2 cm) in the center of the event and a large number ($\sim$ 2,000) of showers, scattered over an area of the diameter $\sim$ 30 cm outside the halo. Preliminary analysis reveals that the estimated energy of the halo is 4.8×10^{16} eV, which is the largest energy of the halo ever observed by emulsion chambers. It is a young air shower or the core of a large air shower.

This paper presents the preliminary analysis of the event, in comparison with the event ANDROMEDA of the comparable energy, which is observed in 1969 by the emulsion chamber at Mt. Chacaltaya by Brazil-Japan collaboration.[1)]

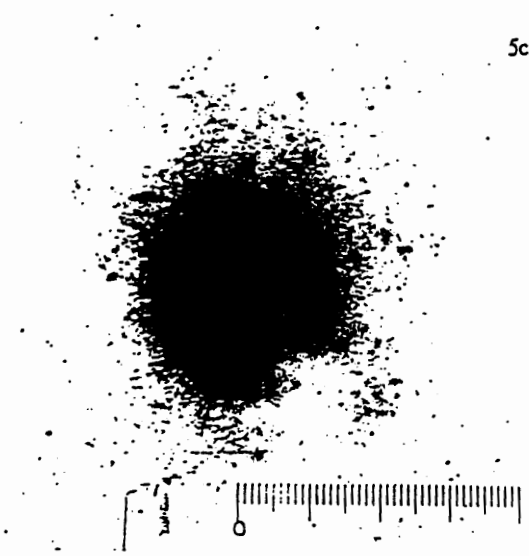

Fig. 1 Photograph of TADJIKISTAN on the X-ray film, inserted at 12 c.u. in Γ-block. The scale is 4 cm. It consists of the halo (the total energy = 4.8×10^{16} eV) in the center and $\sim$ 2,000 high energy showers outside the halo.

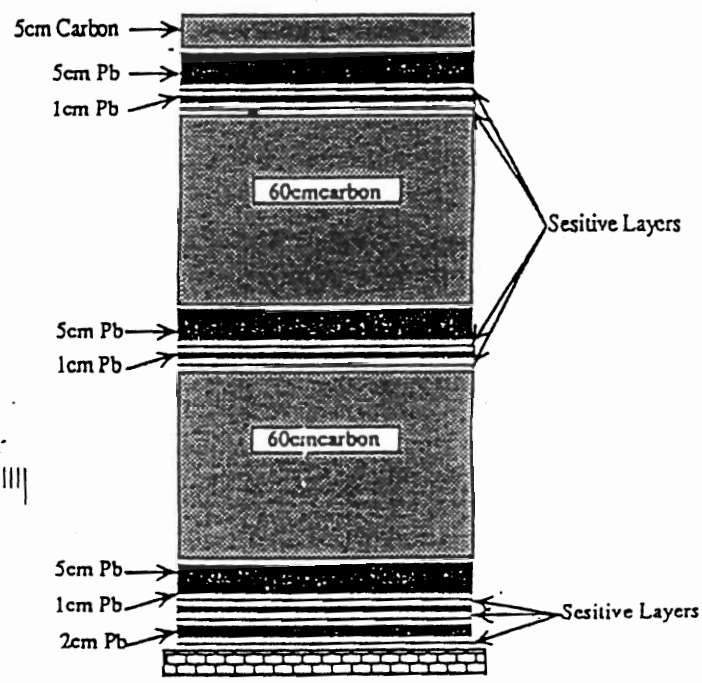

Fig. 2 Structure of the emulsion chamber at Pamirs.

II. Experimental Procedure.

(1) Emulsion chamber at Pamirs.

Emulsion chamber is three storied type (Γ, H1 and H2 block) with two producer layers (60 cm C) in between. Each producer is equivalent to 1.2 inelastic collision mean free path of nucleons. The sensitive layer, inserted at various depths in the chamber, consists of one sheet of X-ray film of high sensitivity. (Fig.2)

Location	Pamirs (4,300 m, 595 g/cm^2, Tadjikistan)
Exposure	
Structure	Producer (5cm C) Emulsion chamber (Γ-block, 6 cm Pb, 2 sensitive layers) Producer (60 cm C) Emulsion chamber (H1-block, 6 cm Pb, 2 sensitive layers) Producer (60 cm C) Emulsion chamber (H2-block, 8 cm Pb, 3 sensitive layers*)
Sensitive Layers	X-ray film RT-6

* The film at the last layer is missing.

The emulsion chamber by which ANDROMEDA is observed is of a simple type; 11 cm Pb with 10 sensitive layers inserted under every 1 cm Pb except the first 1 cm. The sensitive layer consists of three sheets of X-ray film (two of high sensitivity and one of low sensitivity) and one sheet of nuclear emulsion plate, which served much for understanding the halo. Electron tracks can be recognized one by one in the nuclear emulsion plate by the microscope, while a bundle of electron tracks ($> 10^2$) is visible by a naked eye as a small dark spot on the X-ray film.

(2) Performance of emulsion chamber.

Emulsion chamber, a multiple sandwich of sensitive layers and lead plates, detects the electron showers of high energy (> several TeV), produced in the chamber by high energy cosmic-ray particles incident upon the chamber.

An electromagnetic particle (i.e. e or γ, called a γ-ray hereafter) incident upon the chamber produces an electron shower in the chamber through the cascade process of electromagnetic interactions in lead plates. The electron shower makes a small dark spot ($\sim$ 100 μm), visible by a naked eye, on the X-ray films after photographic development. Hence the sensitive layers, inserted at various depths in the chamber, observe the various stage of shower development. The photometric measurement of the shower spot enables us to determine the energy of the γ-ray with the aid of the cascade theory. Thus the emulsion chamber determines the energy and position of the incident particle. The detection threshold of the emulsion chamber is several TeV, depending on the sensitive materials, the structure of the chamber, the condition of the exposure, etc.

A hadron incident upon the chamber gives rise to nuclear interactions in the producer layer and/or in the lead plate, and the electromagnetic component (mainly from the decays of π^0's) among the produced particles originates an electron shower in the chamber. Hence the detection of hadrons depends on the collision probability in the chamber, the energy fraction of electromagnetic component produced in the interaction (i.e. $k_\gamma \equiv \Sigma E_\gamma / E_h$), and the detection threshold. And the observed energy of the hadron-induced shower $E_h^{(\gamma)}$ is not the energy of the incident hadron E_h but a fraction of it, i.e. $E_h^{(\gamma)} = k_\gamma E_h$.

(3) Event TADJIKISTAN

Photometric measurement is made by a microphotometer with the slit size of $200\mu m \times 200\mu m$. X-ray film has two emulsion layers, coated on both sides of plastic base, but one side of emulsion layer is stripped off for those of this event because otherwise opacities are too high for measurement.

(3-1) *Halo.*

It is known by the microscopic observation of nuclear emulsion plates, which is possible for ANDROMEDA, that the halo is made of a large number of electrons distributed continuously.

The darkness distribution of the halo is obtained by the step-wise raster scanning of the microphotometer, over the area of 5 cm × 5 cm containing the halo. Then the darkness D is converted to the electron density ρ (electrons/cm^2) by the characteristic curve of the X-ray film,

$$D = D_0 \, (1 - e^{-\alpha\rho})$$

where $D_0 = 4.0$ and $\alpha = 3.25$ (μm^2).

The lateral distribution of electron density $\rho(r)$, thus obtained, is integrated with respect to r to obtain the total electron number N_e in the halo. The transition curve of N_e is given in Fig. 3, which shows that TADJIKISTAN has larger number of electrons in the large depth of the chamber than ANDROMEDA, indicating that TADJIKISTAN is rich in hadrons, compared with ANDROMEDA.

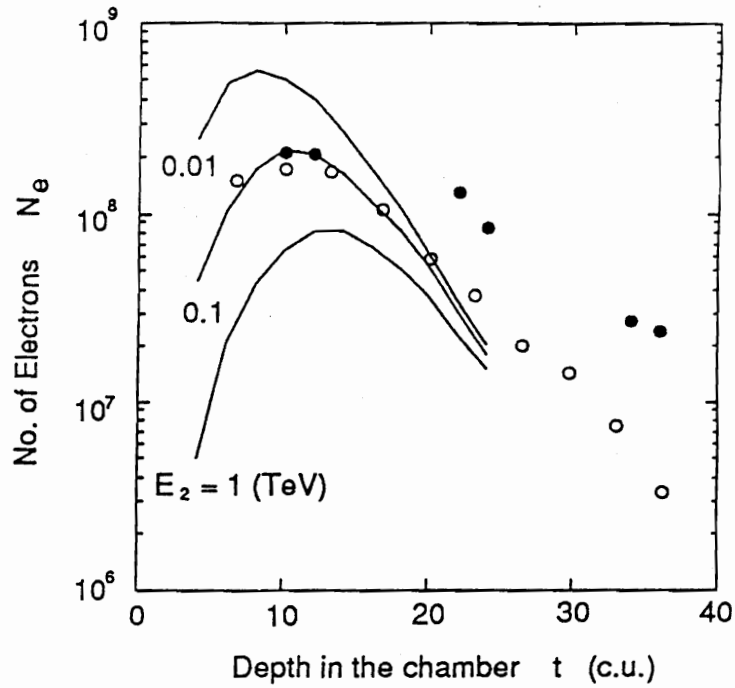

Fig. 3 Transition curve of the total electron number in the halo. (• TADJIKISTAN, o ANDROMEDA) See the text in §III (1) for the solid curves.

The total energy of the halo, estimated from the total track length of the halo is 4.78×10^{16} (eV) assuming the critical energy $\epsilon = 7.4$ (MeV) in Pb. (*c.f.* 2.1×10^{16} eV in ANDROMEDA.)

(3-2) *High Energy Showers.*

Many high energy showers are visible outside the halo. It is known by observation in the X-ray films of low sensitivity and in nuclear emulsion plates, possible in ANDROMEDA, that there exist many showers inside the halo, too.

(3-2-1) Identification of showers.

High energy cosmic-ray particles, belonging to the same event, have the same directions of incidence. Therefore we can identify the showers as those of TADJIK-

ISTAN if the configuration of the spots on one film coincides with that on the other film of the same block. We can find that some showers have the continuation to the lower block(s), too.

(3-2-2) Classification of showers.

Classification of showers into γ-induced ones and hadron-induced ones (called γ-rays and hadrons, respectively) can be made by the starting point of the shower, because a γ-ray and a hadron have much different interaction lengths in Pb, 0.57 cm and 18.5 cm, respectively. That is, the showers which starts from Γ-block are identified as γ-rays, if they have no continuation to H1 or H2 block or if, in case of continuation, the energy in Γ-block is larger than that in H1-block. And the showers in all the cases else are identified as hadrons. (See the table below.)

Identification	γ-ray	hadron
Shower of no continuation	Γ	H1, H2
Shower of continuation	Γ-H1 ($E_\Gamma > E_{H1}$)	Γ-H1 ($E_\Gamma < E_{H1}$), Γ-H2, H1-H2, Γ-H1-H2

(3-2-3) Energy determination of showers.

Each block of Γ, H1 and H2 has two X-ray films, inserted at the different depth in the chamber. The energy of the shower is determined by fitting the two plots of darkness vs. depth to the curves which are calculated on the basis of the cascade theory and the characteristic curve of the X-ray film.

Energy spectra of γ-rays and hadrons, outside the halo ($r \geq 1$ cm), are shown in Fig. 4. Fig. 5 presents the energy spectra of γ-rays, inside and outside the halo, of ANDROMEDA.

III. Discussion.

(1) Halo and high energy showers.

In order to see what is the halo, we assume that the halo is produced by the γ-rays which have the energy spectrum,

$$N_0\gamma\left(\frac{E}{E_1}\right)^{-\gamma-1}\frac{dE}{E_1} \qquad (E > E_2,\ \ E_1 = 10.0\ \text{TeV}). \tag{1}$$

Then the transition curve of the total electron number of the halo $N_e(t)$ is given by

$$N_e(t) = \gamma N_0\left(\frac{E_1}{E_2}\right)^{\gamma}\frac{1}{2\pi i}\int\frac{ds}{s}\frac{1}{\gamma - s}\left(\frac{E_2}{\epsilon}\right)^{s} H_1(s)\, K_{1,0}(s,-s)\, e^{\lambda_1(s)t} \tag{2}$$

where all the notations are familiar in the cascade theory.[2] The lower limit of the energy spectrum E_2 governs the depth at the shower maximum, and the index γ the attenuation after the maximum, of the transition curve.

The solid lines in Fig. 3 present the calculated curves of eq.(2). Both TADJIKISTAN and ANDROMEDA may be fitted by the same curve with $E_2 = 0.1$ (TeV) and $N_0 = 8.8\times 10$. The excess of the experimental data over the calculated curve at $t > 20$ (c.u.) is due to the hadrons. The corresponding energy spectrum eq.(1) is shown in Fig. 4 and Fig. 5 in integral form. In the case of ANDROMEDA, a good agreement

is found between the estimated and the observed energy spectrum, showing that the halo is produced by the high energy showers observed in the halo region.

In the case of TADJIKISTAN, high energy showers are visible only outside the halo ($r \geq 1$ cm), but not inside the halo due to the absence of nuclear emulsion plate. One sees in Fig. 4 that the showers outside the halo have larger energies than the energy spectrum of the showers in the halo, expected from the transition curve of N_e. It may indicate that the energies of the high energy showers are somewhat overestimated. The calibration of the energies of the showers will be discussed elsewhere.

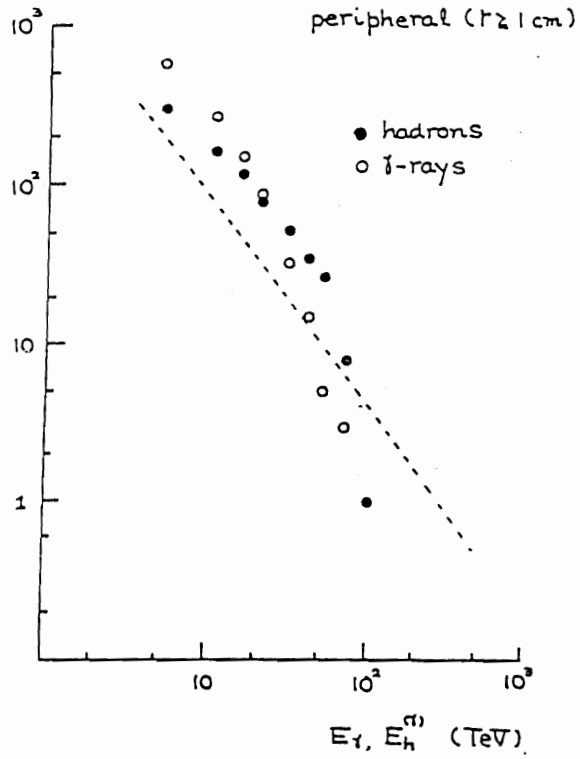

Fig. 4 Energy spectrum of high energy showers, outside the halo ($r > 1$ cm), of TADJIKISTAN. See the text in §III (1) for the dashed line.

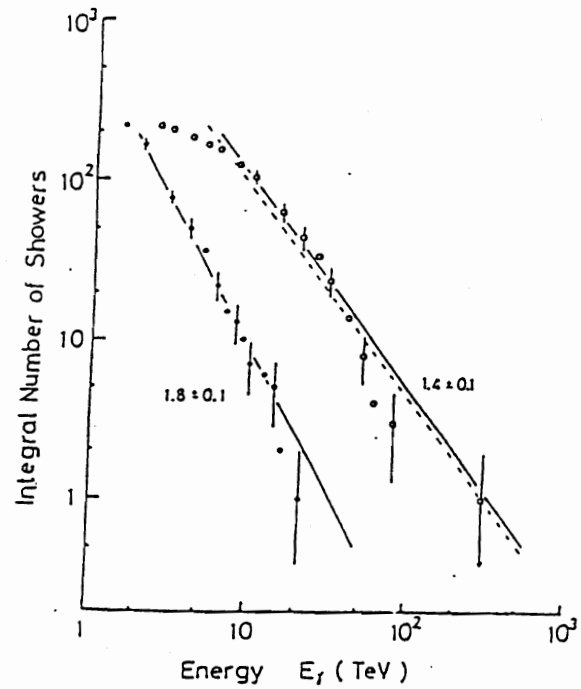

Fig. 5 Energy spectrum of high energy γ-rays, inside (o) and outside (•) the halo ($r_c = 2$ cm), of ANDROMEDA. See the text in §III (1) for the dashed line.

(2) Mean free path of hadrons.

It is reported by the Pamir thick lead chamber experiment that the observed attenuation mean free path (m.f.p.) of hadrons is shorter than the value expected by the ordinary hadrons in the high energy region of $\Sigma E_\gamma > 700$ TeV.[3] TADJIKISTAN is a suitable event to discuss the issue, because of the much higher primary energy, large statistics of hadrons in one event, and large thickness of the chamber.

Fig. 6 presents the number of hadrons outside the halo ($r \geq 1$ cm), observed in H1 and H2 block of the chamber. The chamber depth is measured by inelastic collision m.f.p. of nucleon in C, $\lambda_p = 49.9$ cm (at 200 GeV). The observed attenuation m.f.p. of hadrons is,

$$\frac{\Lambda}{\lambda_p} = 1.41 \; {}^{+0.21}_{-0.32}$$

for the hadrons with $E_h^{(\gamma)} > 10$ TeV.

Fig. 7 presents the dependence of the attenuation m.f.p. on the inelasticity of hadron interaction. The above experimental data with the error is expressed by the hatched area in the figure, because the inelasticity is unknown. The attenuation m.f.p. of nucleon is given by

$$\frac{1}{\Lambda} = \frac{1 - <(1-K)^{\gamma}>}{\lambda_p/1.47} \tag{3}$$

where the factor 1.47 is due to the cross section increase with energy, assuming $< E_h >$ $= 100$ TeV for $E_h^{(\gamma)} > 10$ TeV. And furthermore $\lambda_\pi/\lambda_p = 1.45$ is assumed for the attenuation m.f.p. of pions.

The observed value of the attenuation m.f.p. is compatible with that of pions, which are assumed to be the major part of the hadrons in the cosmic-ray event.

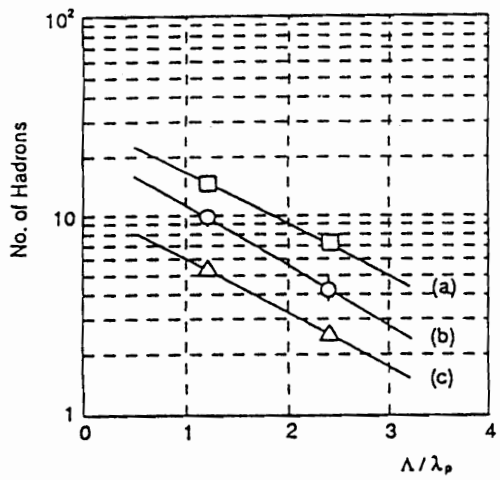

Fig. 6 Number of hadrons, outside the halo ($r > 1$ cm), observed in H1 and H2 block: (a) $E_h^{(\gamma)} > 5$ (TeV), (b) $E_h^{(\gamma)} > 10$ (TeV), (c) $E_h^{(\gamma)} > 20$ (TeV). The chamber depth is measured by the inelastic collision mean free path of nucleon in carbon, $\lambda_p = 49.9$ cm.

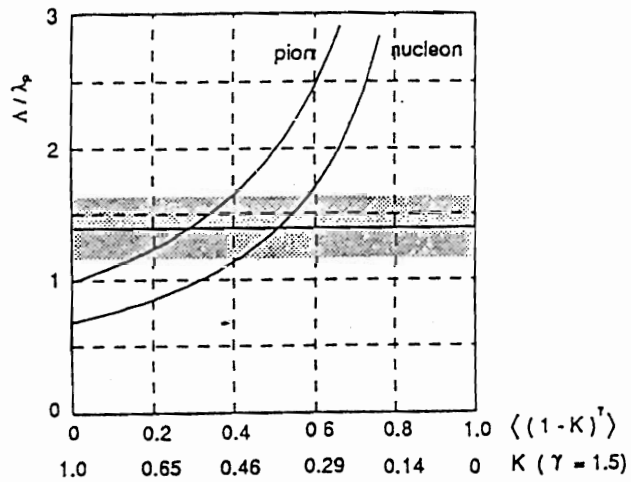

Fig.7 Attenuation mean free path of hadrons and the inelasticity of hadron interactions. Experimental data is shown by the hatched area. See the text in §III (2) for the solid curves of "nucleon" and "pion".

The event was lent out for measurement to Japanese group by Prof. I. Bobodjanov (Institute of Physics and Engineering, Tadjikistan), and the measurement and a preliminary analysis were made by K. Funatani for his Master Thesis of Waseda University.

Reference.

1) S. Yamashita et al., ICR-Report 112-83-6 (1983) (ICRR, Univ. of Tokyo).
2) J. Nishimura, Handbuch der Physik, Vol.XLVI/2 (1967) 1.
3) T. Arisawa et al., Nucl.Phys. B424 (1994) 241.

Comments to Short Mean Free Path Particles Observed by Pamir Thick Lead Chambers

Akinori Ohsawa, Carlos E. Navia* and Edison H. Shibuya†

Inst. for Cosmic Ray Research, University of Tokyo, Tanashi, Tokyo, Japan.

* *Dep. de Fisica, Univ. Federal Fluminense, Niteroi, Rio de Janeiro, Brasil.*

† *Inst. de Fisica, Univ. Estadual de Campinas, Campinas, São Paulo, Brasil.*

I. Introduction.

Arisawa et al. have made an estimate of the interaction mean free path (m.f.p.) of high energy hadrons in Pb through the starting point distribution (s.p.d.) of showers in thick lead-emulsion chambers (60 cm and 120 cm Pb) constructed at the Pamir Cosmic Ray Station.[1)] They reported that the hadrons in the families of $\Sigma E_\gamma \geq 700$ TeV have a m.f.p. for inelastic collisions in Pb as short as $(\frac{1}{2} \sim \frac{1}{3})\lambda_0$, where λ_0 is the m.f.p. for nucleon-Pb inelastic collisions at low energies; $\lambda_0 = 210$ (g/cm^2 Pb) = 18.5 (cm Pb), corresponding to 1,632 (mb). The existence of short m.f.p. hadrons in the high energy region provides a clear-cut explanation for some of the unsettled problems in cosmic-ray physics.[2)]

But, before entering upon a discussion of the physical significance of the reported short m.f.p. hadrons, we will try in this paper to study in detail the behavior of hadrons in the chamber. This will clarify simultaneously which physical quantities relate to the observed s.p.d. of showers, and to what extent the distribution is explained by the conventional physical processes, etc.

II. Experimental Procedure.

(a) Emulsion chamber.

Emulsion chamber is a detector, consisting of photo-sensitive layers (X-ray films, nuclear emulsion plates) and lead plates which are piled up alternately. It detects an electron shower, whose energy is determined by the cascade theory. The emulsion chamber has a high threshold for shower detection, say $E_{th} = 1 \sim$ several TeV in terms of shower energy. Therefore, all the showers, produced in the chamber, are not necessarily detected.[2)]

A hadron, incident upon the chamber, makes nuclear interaction(s) in the chamber to produce electron shower(s). And the estimated energy of the shower is a part of the incident energy of the hadron, because k_γ (the ratio between the energy to produce the shower and that of the incident hadron) is smaller than one.

(b) Attenuation length of the starting point distribution of showers.

The energy and the starting point of the shower are determined at the same time by fitting the transition curve of the shower to those of the cascade theory.

When the shower curve shows a complicated behavior (of double peaks, etc., mainly due to the successive interactions), impossible to be fitted to the smooth curve of the cascade theory, the four data points around the maximum are used to estimate the energy and the starting depth. Showers of successive interactions are treated as different showers, when they are well separated.

The s.p.d. is constructed for showers of "single" and "family". The former are the showers of isolated incidence, while the latter are the members of the family where a bundle of showers have the same direction of incidence. The family is produced through the cascade processes, nuclear and electromagnetic, in the atmosphere.

We obtain the attenuation length Λ by fitting the s.p.d. to the function, $\exp(-t/\Lambda)$ where t is the depth of the chamber.

Attenuation length is discussed for the showers which have starting points deeper than 10 cm Pb in the chamber. Those showers cannot be produced by the electromagnetic component ($e^{\pm}, \gamma$) which have an interaction m.f.p. $X_0 = 0.57$ cm Pb in the chamber. Hence the particles to produce these showers are called "hadrons" tentatively.

Table 1 Attenuation length of starting point distribution

Λ (g/cm^2)	γ	E_{min} (TeV)	$< E >$ (TeV)	$\lambda(E)$ (g/cm^2)	$\frac{\Lambda}{\lambda(E)}$	$\frac{E_{th}}{E_{min}}$
$\Lambda_f = 146 \pm 40^a$	1.2	20	416	176	0.83 ± 0.23	0.15
$\Lambda_f = 176 \pm 48^b$	1.2	10	208	178	0.99 ± 0.27	0.30
$\Lambda_f = 144 \pm 18^c$	1.2	4	138	180	0.80 ± 0.10	0.75
$\Lambda_s = 252 \pm 30$	2.1	6	58.9	182	1.38 ± 0.16	—
$\Lambda_s = 251$ (22 cm)	1.8	2	24.0	184^d	1.36	—

[a] 17 families (68 hadrons with $E > 20$ TeV) with $\Sigma E_\gamma > 700$ TeV.

[b] 17 families (143 hadrons with $E > 10$ TeV) with $\Sigma E_\gamma > 700$ TeV.

[c] 40 families (119 hadrons with $E > 4$ TeV) with $\Sigma E_\gamma = 100 \sim 500$ TeV.

[d] 14 (cm) = 159 (g/cm^2) is concluded by the authors.[3)]

Table 1 shows the attenuation lengths, Λ_s and Λ_f, the exponent of the integral energy spectrum, γ, and the minimum energy of the showers, given in Refs. 1) and 3). $< E >$ in the table is the average energy of nucleons, given by

$$< E >= \frac{\gamma}{\gamma - 1}\frac{E_{min}}{a} \quad \text{with} \quad a = \left[\int k_\gamma^\gamma dk_\gamma\right]^{1/\gamma} = \frac{c}{(\gamma+1)^{1/\gamma}} \tag{1}$$

and $\lambda(E)$ is the m.f.p. of inelastic nucleon-Pb collisions by Glauber theory, corresponding to $< E >$ of nucleons. $\Lambda/\lambda(E)$ is the value to be compared directly one another, because each set of data consists of the showers of different energy region.

The two values of Λ_s by Pamir[1)] and Fuji[3)] experiments are consistent with each other, and Λ_f's[1)] are appreciably smaller than Λ_s.

III. Attenuation Length of Starting Point Distribution of Showers.

In this section we will derive the starting point distribution of showers to get the attenuation length on the following assumptions:

(1) the incident hadrons are nucleons with the energy spectrum $\gamma N E_0^{-\gamma-1} dE_0$.

(2) the inelasticity K in nucleon-Pb collision is assumed uniform between 0 and 1.

(3) k_γ is given by $k_\gamma = cK$ with $c = 1/3$.

The number of nucleons at the depth t in the chamber is given by,

$$F(E,t)dE = \gamma N E^{-\gamma-1} dE \sum_0^\infty \frac{1}{n!}\left(\frac{t}{\lambda}\right)^n \exp\left(-\frac{t}{\lambda}\right) \times \int (\eta_1\eta_2\cdots\eta_n)^\gamma \, d\eta_1 d\eta_2 \cdots d\eta_n \tag{2}$$

where η is the elasticity, assumed to be uniform. The integration regions of η's, which specify nuclear interactions between $0 \sim t$ of the chamber, are determined by the experimental condition. The s.p.d. is obtained from $F(E,t)$ easily.

(i) Attenuation length of single showers.

Suppose that a nucleon makes a visible shower at the depth t in the chamber. It doesn't specify anything about the nuclear interactions between 0 and t in the case of single showers. That is, there may or may not be visible showers between 0 and t, and the integration regions are $0 \sim 1$ for all the η's. Then we have,

$$\frac{1}{\Lambda_s} = \frac{1}{\lambda}\left[1 - \frac{1}{1+\gamma}\right] \tag{3}$$

which is shown in Fig. 1. Λ_s is the same as the attenuation length of nucleons in the atmosphere.

(ii) Attenuation length of the first starting point, Λ_{1st}.

Suppose that a nucleon makes the *first* visible shower at the depth t in the chamber. It specifies that the nucleon did not make any visible showers between 0 and t of the chamber. That is, all the nuclear interactions between 0 and t produce the showers whose energies are below the detection threshold. The integration regions are $\eta = 1/(1+b) \sim 1$ with $b = E_{th}/cE$ for all η's.

The attenuation length Λ_{1st}, calculated on the above consideration, is shown in Fig. 1 for various values of observation depth ($t/\lambda = 2, 10$) and the minimum shower energy ($E_{th}/E_{min} = 1.0, 0.5, 0.1$). It depends reasonably on E_{th}/E_{min}, but slightly on t/λ. And it is natural that Λ_{1st} approaches λ as $E_{th}/E_{min} \to 0$ and Λ_s as $E_{th}/E_{min} \to \infty$, and that Λ_{1st} is appreciably smaller than Λ_s.

IV. Discussions.

(i) One of the reasons for the remarkable difference between Λ_s and Λ_f in Table 1 may be due to the identification of the family. That is, the family is identified when plural number of showers have the same direction and inclination of incidence on the shower map where showers are projected on horizontal plane. However, it is not so easy to make a precise map for the showers located deep in the chamber, because there is not always the reference showers deep in the chamber. These family showers which may have a slightly different direction of incidence from other members of the family on the map due to the error of the map, are possibly not identified as the family members. Consequently Λ_f is approximately equal to Λ_{1st}.

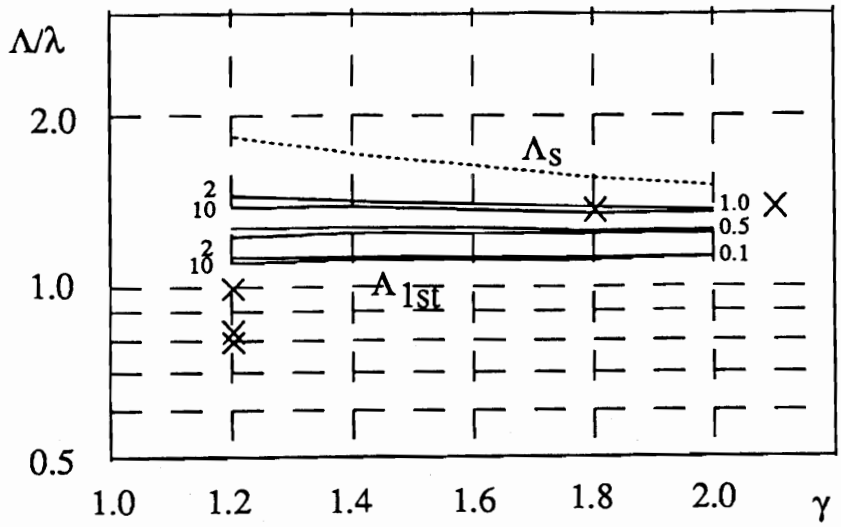

Fig. 1. Attenuation length of the shower starting points, normalized by the mean free path of nucleon-Pb collision. γ of the ordinate expresses the exponent of the energy spectrum of the observed showers. The dotted line and solid lines are for Λ_s and Λ_{1st}, respectively. The figures, attached to the curves of Λ_{1st}, are the observation depth (t/λ) on the left and the minimum energy of the shower (E_{th}/E_{min}) on the right. The crosses $(\times)$ are the experimental data in Table 1.

(ii) Fig. 1 shows that Λ_s of the calculation is larger than the experimental data. Let us examine the possibility that the average inelasticity has a larger value in nucleon-Pb interactions than $< K >= 0.5$ assumed in the present analysis. If we want to get $\Lambda_s/\lambda = 1.35$, we must have $< (1-K)^\gamma >= 0.26$. It follows $< K >= 0.61$ for $\gamma = 2.0$, assuming a flat distribution of K between a $(\neq 0)$ and 1.

It may be worthy to add that the calculated curves of Λ_{1st} also go down closer to the line of $\Lambda_{1st}/\lambda = 1.0$ for larger values of the average inelasticity.

References.

1) T. Arisawa et al., Nucl. Phys. **B424** (1994) 241.
2) C.M.G. Lattes et al., Phys. Rep. 65 (1980) 151.
3) M. Akashi et al. (Mt. Fuji Collaboration), Nuovo Cim. 65A No.3 (1981) 355.

Nuclear Interaction Families Associated to EAS at Mt. Chacaltaya

N. Kawasumi, I. Tsushima, K. Honda, K, Hashimoto, T. Matano [1],
N. Inoue [2], K. Mori [2], K. Yokoi [3], A. Ohsawa [4], M. Tamada [5], N. Ohmori [6],
N. Martinic [7], R. Ticona [7], N. Gironda [7] F. Osco [7] and C. Aguirre [7]

Department of Physics, Yamanashi University, Kofu 400, Japan.
[1] *Dep. of Applied Phys. and Chem., Fukui Inst. of Technology, Fukui 910, Japan.*
[2] *Department of Physics, Saitama University, Urawa 338, Japan.*
[3] *Fac. of Sci. and Eng., Aoyama Gakuin University, Setagaya, Tokyo 157, Japan.*
[4] *Inst. for Cosmic Ray Research, University of Tokyo, Tanashi, Tokyo 188, Japan.*
[5] *Fac. of Science and Technology, Kinki University, Kowakae, Osaka 577, Japan.*
[6] *Department of Physics, Kochi University, Kochi 780, Japan.*
[7] *Inst. de Inv. Fisicas, Universidad Mayor de San Andres, La Paz, Bolivia.*

1. Introduction.

Observation of high energy cosmic-ray phenomena is made at Mt. Chacaltaya (5,200 m, Bolivia) by operating the emulsion chamber (EC) and the air shower (AS) array simultaneously. EC of 8 m^2 of area and 15 cm thick, located in the center of the AS array, observes the family, a bundle of high energy particles, electromagnetic (called "γ-rays") and hadronic, in the phenomenon. The burst detectors are installed under EC to find the correspondence between the family and the accompanying AS. The AS array consists of 44 scintillation detectors of 0.25 m^2 and 1 m^2, distributed over the area of 50 m in radius, and of 8 fast-timing detectors. The former measure the lateral distribution of electron density, which determines the total size N_e and the age s of AS, and the latter the arrival direction of AS.

Total exposure of EC is 41.2 m^2·yr up to date, and 47 families, fulfilling the criteria (1) the threshold energy of the shower $E_{th} > 2$(TeV), (2) the number of γ-rays $n_\gamma \geq 5$, and (3) the total energy of γ-rays $\Sigma E_\gamma \geq 10$(TeV), are connected with the accompanying AS's. The coupling rate is 70 % out of the total recorded families.

Simultaneous observation of the family and the accompanying AS has several advantages, compared with the respective experiments of EC and AS array. For example, the experiment can give an answer to the long-standing controversy — the change of the nuclear interactions *or* the increase of the heavy nuclei in the primary cosmic rays —, regarding the cause of the strong attenuation of cosmic rays in the atmosphere.

In this paper we will present a summary of the experimental results in §II, and a description of some individual events of particular interest in §III.

2. Summary of the experimental results.

We present a brief summary of the experimental results, because the detailed discussion was given elsewhere.[1)]

Simulation calculation [2)] for comparison assumes UA5 simulation algorithm [3)] for the hadron interactions and a normal composition for the primary cosmic rays. The former reproduces the features of multiple particle production, observed mainly by UA5 collaboration,[3)] and assumes a mild violation of Feynman scaling law in terms of $(1/\sigma_{inel})d\sigma/dx$ with $x = E/E_0$. The latter assumes the energy spectrum of $E^{-1.8}$ in integral form with the composition of p : 42 %, He : 17 %, CNO : 14 %, heavy : 14 % and Fe : 13 % at 10^{15} eV, which is an extrapolation of the experimental data in low energy region where the direct measurement is possible.

(1) The size spectrum of all the AS's and ΣE_γ spectrum of all the families are in agreement with those by BASJE [4)] and Brazil-Japan EC Collaboration [5)] which are the experiments carried out at the same site. It assures the consistency of the experiments one another.

(2) Energy spectrum of γ-rays and hadrons in the family.

The energy spectra of gamma-rays in the family for three bins of the AS size ($N_e = 10^5 \sim 10^6 \sim 10^7 \sim 10^8$) are compared with the simulation, showing that the slopes of the spectra agree with each other while the number of gamma-rays in one family is smaller in the experimental data than in simulation.

The experiment HADRON at Tien-Shan[6)], the same type of experiment as the present one, reported that the slopes of energy spectra of gamma-rays become steeper in the size region exceeding 10^7. And they discuss the change of the characteristics of nuclear interactions in the region above 10^{16} eV. Such a change, however, is not found in the present experiment.

The energy spectra of γ-rays and hadrons in the same range of ΣE_γ agree one another independently of N_e. It indicates that the family is produced deep in the atmosphere mainly by one of the high energy hadrons in AS, and therefore there is no strong correlation between N_e and the energy spectrum of gamma-rays in the family. It doesn't mean, however, that the information of AS is useless for family analysis, which will be shown below in many examples.

The energy spectra of gamma-rays for four ranges of ΣE_γ ($10 \sim 21.5 \sim 46.4 \sim 100 \sim 215$ TeV) irrespectively of the AS size, agree with the simulation both in the spectral index and in the number of gamma-rays. It is the case for the energy spectra of hadrons, too.

In summary the simulation does reproduce the features of the family well, but does not the relation between the air shower (or the primary energy) and the family.

(3) Correlation between ΣE_γ and N_e.

Figure 1 shows the scatter plot of ΣE_γ of the family and N_e of the accompanying AS. And Figure 2 shows the average value of ΣE_γ vs. N_e by the experiment and by the simulation. It is clearly seen in Fig. 2 that the experimental data do agree with the simulation in the lower size region, but do not in the higher size region.

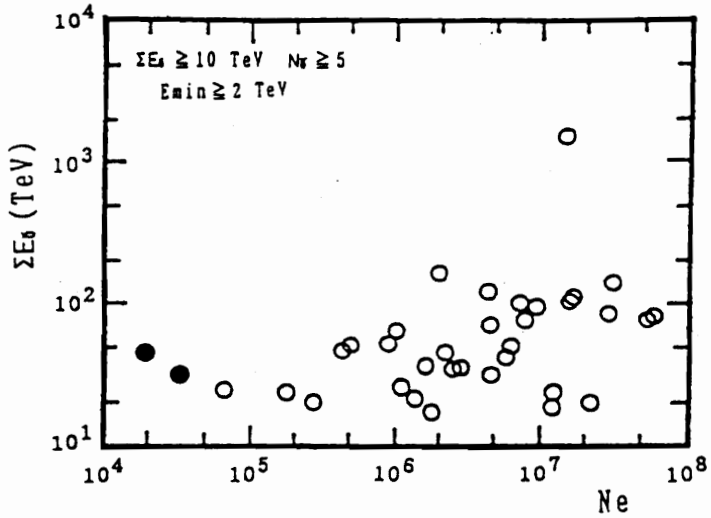

Fig.1 Correlation between ΣE_γ (the total energy of γ-rays in the family) and N_e (the size of the accompanying air shower). See §III for the full circles.

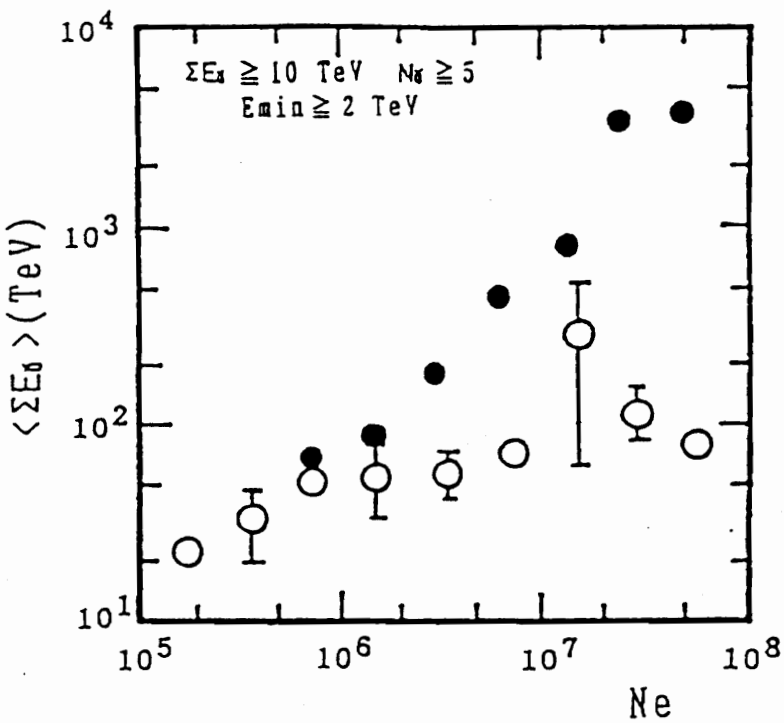

Fig.2 Average value of ΣE_γ and N_e.
o : experiment
• : simulation

The discrepancy indicates a necessity of more rapid energy-dissipating process in the atmosphere than those assumed in the simulation. Possibilities for such a process under discussion are the increase of heavy component in the primary cosmic rays (e.g. iron component) and the change of nuclear interactions (e.g. the violation of Feynman scaling law in multiple particle production, the existence of the exotic events, etc.).

The simulation, however, shows that $< \Sigma E_\gamma >$ decreases slightly even when the large fraction of iron nucleus is assumed in the primary cosmic rays, because mainly protons produce families in low energies and both protons and irons produce families of large ΣE_γ in high energies.

3. Clean families.

One of the advantages of the simultaneous observation is the possibility to select the events of low production height. It is sure that these events are produced by nucleons penetrating deep in the atmosphere and preserve the features of high energy interaction without suffering the cascade degradation through the atmosphere.

We select two events of larger value of $\Sigma E_\gamma / N_e$ (the full circles in Fig. 1) for such candidates. Really the events have small ages s of the accompanying AS's. (See Table 1.)

Table 1 : Candidate events of low production height.

Name	ΣE_γ (TeV)	$\Sigma E_h^{(\gamma)}$ (TeV)	$< E_\gamma \times r >$ (TeV · cm)	N_e	s	H (m)
0918X-50	43.5	0	1.98×10	1.95×10^4	0.29	990
B21-22D	32.5	19.6	3.64×10^{-2}	3.76×10^4	0.40	1.8

The analysis of the events is made on the assumption that the family and the accompanying AS are produced from the same interaction. The production height H is estimated from $< E_\gamma \cdot r >$ of the family, assuming $< p_{T\gamma} >= 0.2$ (GeV/c). The production height of the event B21-22D is unrealistic, indicating that the event has smaller $< p_{T\gamma} >$. Taking into account the existence of hadrons in this event, it is a good example of "mini-cluster", reported by Brazil-Japan EC Collaboration.[7)]

The radiated energy of the event 0918X-50, $E_0 = 3.0 \times 10$ (TeV), estimated from the s and H, is consistent with ΣE_γ.

Reference.

1) Kawasumi N. et al., AIP Conf. Proc. **276** (1992) 88, and Proc. VIII Intern. Sympo. on Very High Energy Cosmic Ray Interactions (1994) 283.
2) Tamada M., Proc. Int. Workshop on Super-High Energy Hadron Interactions (1991) 263, and 7th Int. Sympo. on Very High Energy Cosmic Ray Interactions, AIP Conf. Proc. 276 (1992) 126.
3) UA5 Collaboration (Alner G.L. et al.), Nucl. Phys. B291 (1987) 445.
4) Suga K. et al., 16th Int. Cosmic Ray Conf. 13 (1979) 142.
5) Baradzei L.T. et al., Nucl. Phys. B370 (1992) 365.
6) Arabkin V.V. et al., 22nd Int. Cosmic Ray Conf. Vol.4 (1991) HE-1.2.32, HE-1.3.6 and HE3.1.5.
7) Lattes C.M.G., Fujimoto Y. and Hasegawa S., Phys. Rep. **65** (1980) 152.

Violation of the Feynman Scaling Law in the Forward Region

A. Ohsawa
Institute for Cosmic Ray Research, University of Tokyo,
Tanashi, Tokyo, 188 Japan.

1. Introduction

Feynman scaling law[1] regarding the inclusive energy spectrum of produced particles in multiple particle production, seemed to be valid in the energy region $\sqrt{s} \leq 63$(GeV).[2] It is important to establish whether it holds or not in still higher energy region, because the energy spectrum of produced particles is one of the important features to be satisfied by models of multiple particle production. Furthermore how much the law is violated in the forward region at high energies is crucial for the analysis of high energy cosmic-ray phenomena, in particular those observed deep in the atmosphere, because the nuclear cascade process in the atmosphere plays a decisive role to the phenomena. For example, among topics of current interest, it is closely related to the estimation of heavy nuclei content in primary cosmic rays, the energy estimation of extensive air showers, the flux estimation of atmospheric neutrinos, the possibility to discriminate γ-induced showers from proton-induced ones, etc.

We will discuss the scaling law in terms of $dN/dx^* = (1/\sigma_{inel})d\sigma/dx^*$ where $x^* = 2p_{\parallel}^*/\sqrt{s}$. (The quantities with an asterisk are those in CMS.) It is almost identical to discuss the subject in terms of dN/dy^* or $dN/d\eta^*$ where y^* and η^* are rapidity and pseudo-rapidity, because we have $dN/dy^* \simeq dN/d\eta^* \simeq x^* dN/dx^*$ approximately.

There exist three sets of data to discuss the subject in the forward region of the collision in high energy region; (1) $dN/d\eta^*$ of charged particles ($\eta^* < 4.5$) at $\sqrt{s} =$ 53, 200, 546 and 900 (GeV) at CERN S$\bar{p}$pS collider by UA5 Collaboration,[3] (2) dN/dy^* of π^0's ($5.0 < y^* < 6.5$) at $\sqrt{s} = 630$ (GeV) at CERN S$\bar{p}$pS collider by UA7 Collaboration,[4] and (3) $dN/d\eta$ of γ-rays ($\eta > 1.0$) at $< \sqrt{s} >= 500$ (GeV) from C-jet observation by Brazil-Japan Collaboration of cosmic-ray experiment at Mt. Chacaltaya.[5]

Conclusion on the validity of the scaling law is different by respective groups above, but there is no cross-examination of three sets of data because comparison of the data is not straightforward due to the fact that each set of data is expressed by different physical quantity owing to their experimental conditions. The present work is the first that tries to examine them in a unified way of analysis.

In § II we will present an analysis of three sets of data, made on the assumption that all the produced particles are pions, and in § III correction factors to dN/dx, obtained in § II, due to the composition of produced particles and the *possible* effect

of the projectile charge. § IV is devoted to the discussions on the consequences of the violation of the Feynman scaling law.

2. Analysis

In order to analyze the data which are expressed by the different physical quantity by respective groups, we introduce two-dimensional distribution,

$$\frac{d^2N}{dy^* dp_T} = f(y^*)\, g(p_T)\,, \tag{1}$$

where $g(p_T) = p_T \exp(-p_T/p_0)/p_0^2$. p_0 is *dependent* on y^* so that $< p_T >$ has a rapidity dependence to decrease in the forward region and to agree with UA7 data at $\sqrt{s} = 630$ (GeV). The equation (1) can be rewritten easily as,

$$\frac{d^2N}{d\eta^* dp_T} = f(y^*)\, g(p_T) \frac{p_T \cosh(\eta^*)}{\mu \cosh(y^*)} \qquad (\mu \sinh(y^*) = p_T \sinh(\eta^*)) \tag{2}$$

$$\frac{d^2N}{dx^* dp_T} = f(y^*)\, g(p_T) \frac{1}{\sqrt{x^{*2} + \left(\frac{2\mu}{\sqrt{s}}\right)^2}} \qquad (x^* = \frac{2\mu}{\sqrt{s}} \sinh(y^*)) \tag{3}$$

where $\mu = \sqrt{{p_T}^2 + m^2}$ (m : pion mass).

The analysis is made on the simplified assumption of,

(1) all the produced particles are pions,

(2) π^+'s, π^-'s and π^0's have the same distribution.

We present here only the conclusion of the analysis, because details of the analysis are given already elsewhere.[6)]

(1) The data of $dN/d\eta^*$ from UA5 Collaboration show both the increase of the density in the central region and the *strong* decrease in the forward region, compared with the scaling distribution. However, if ones give less weight to the data points in the region $\eta^* > 4.0$, one may conclude that the scaling law is valid in the forward region. That is the reason why there are different kinds of estimation on the validity of the scaling law in the forward region, based on the same data of UA5 experiment.

(2) The data of dN/dy^* from UA7 Collaboration show the decrease of the distribution in the forward region, compared with the scaling distribution.

(3) The distributions of $dN/d\eta^*$ from UA5 and UA7 Collaborations, which fall on the different pseudo-rapidity intervals, connect smoothly. Hence one can combine both data to construct the empirical distribution of $(dN/d\eta^*)_{UA5+UA7}$ at $\sqrt{s} = 630$ (GeV), valid both in the central and forward regions.

(4) The distribution of dN/dx from Brazil-Japan Collaboration agrees well with $(dN/dx)_{UA5+UA7}$. (See Fig. 1.)

(5) The total inelasticity, obtained from $(dN/dx)_{UA5+UA7}$, amounts to $K = 0.41 \pm 0.05$ at $\sqrt{s} = 630$ (GeV).

3. Correction Factors to dN/dx and K.

We discuss the correction factors to dN/dx and K due to the composition of produced particles and *possible* effect of the projectile charge. The discussion needs further assumptions which are not established well. However, it is meaningful for claiming the violation of the scaling law, because these effects will increase the distribution, resulting the recovery of the scaling law.

The discussion, given below in detail, concludes that the increase of dN/dx is by a factor $1.00 \times 1.3 = 1.3$ in the forward region (at $x = 0.2$). The x-distribution after the correction, shown in Figure 1 by the solid line, still shows an appreciable suppression of particle production in the forward region, compared with the scaling distribution. And the inelasticity is increased by a factor $1.15 \times 1.00 = 1.15$, giving $K(corr.) = 0.47 \pm 0.06$. The corrected value is smaller than 0.5 (of the scaling case), in spite of the increase of the particle density in the central region.

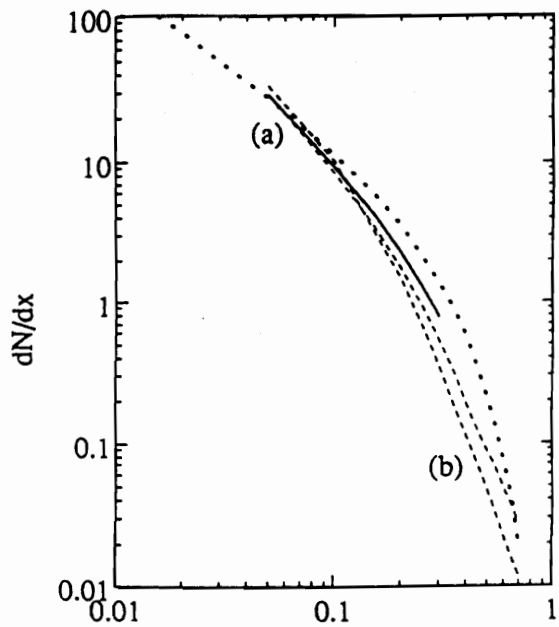

The x distributions. Dashed curve (a) is $dN_{UA5+UA7}/dx$ from the empirical formula of Eq. (19), which reproduces both the UA5 and UA7 data consistently, and (b) is dN_{C-Jet}/dx from the rapidity density distribution of γ-rays based on the C-jet data. The experimental data exist in the region $x<0.3$ for both curves of (a) and (b). Curves (a) and (b) are consistent with each other, and show a smaller density in the forward region, compared with the dotted curve of the scaling function of Eq. (13). The solid line is the corrected distribution of curve (a), taking into account the produced particle composition and projectile charge effect. It shows still an appreciable suppression of the particle production in the forward region.

(1) Composition of produced particles.

Table 1 shows a summary of particle composition (Leading particles are excluded.) in $\bar{p}p$ collisions at $\sqrt{s} = 546$ (GeV) in a non-single-diffractive events, given by the UA5 collaboration.[3] Figures are the average numbers of particles in one event.

Table 1: Particle composition

$\pi^{\pm}$	π^0	η	charged	neutral
22.0	11.0	3.4	26.1	18.7

The π^0's to be observed in the experiment are the sum of those produced directly and those through the decays of the η's, i.e. $\eta \to \pi^0\pi^0\pi^0$ (31.8 %) and $\eta \to \pi^+\pi^-\pi^0$ (23.7 %). Assuming that a half of the π^0's from the η's are observed in the forward region on the rapidity scale, we have

$$n_{\pi^0} = 22.0 + 3.4 \times (3 \times 0.318 + 1 \times 0.237)/2 = 13.0$$

Assuming further that the local particle composition at any rapidity region is the same as the total one, given in Table 1, and that all kinds of produced particles have the same energy spectra, we can discuss the correction factors in the following way.

The correction factor to dN/dx is $n_{charged}/2n_{\pi^0} = 1.00$, and that to K is either $\{n_{charged} + n_{neutral}\}/1.5n_{charged} = 1.15$ or $\{n_{charged} + n_{neutral}\}/3.0n_{\pi^0} = 1.15$ for the cases when it is estimated from charged particles or from π^0's, respectively.

(2) Effect of the projectile charge in the forward region.

According to the data of bubble chamber experiments[7], the following relations exist approximately in the inclusive reaction of $pp \rightarrow \pi + X$:

$$f(x)_{\pi^+} = af(x)_{\pi^-} \qquad \text{and} \qquad f(x)_{\pi^0} = f(x)_{\pi^-}$$

where $f(x) = dN/dx$ and $a = 1.0$ in the central region while $a \simeq 1.2, 1.6, 2.0$ at $x = 0.1, 0.2, 0.3$ in the forward region. It shows that there exists the effect of the projectile charge in the forward region.

Hence, when $f(x)$ of *charged* particles is estimated from that of π^0's,

$$f(x)_{\pi^+\pi^-} = \{2f(x)_{\pi^0}\}\frac{a+1}{2}$$

which shows that the correction factor is 1.1, 1.3 and 1.5 at $x = 0.1$, 0.2 and 0.3, respectively. The correction to K is negligible, because $f(x)$ is enhanced in the central region.

4. Discussion

We have shown that the Feynman scaling law is violated appreciably both in the central and forward regions at high energies of $10^{14\sim15}$ eV, giving very weak decreasing energy dependence of inelasticity. One should keep it in mind that the estimate is made in the way most favored to the scaling law.

It was pointed out that the decreasing inelasticity is compatible with the existence of the exotic events[8], such as Centauro[9], etc.

References.

1) Feynman R. Phys. Rev. Lett. **23** (1969) 1415. 2) Taylor F.E. et al. Phys. Rev. **D14** (1976) 1217. 3) Alner G.L. et al. Phys. Rep. Nos.5/6 (1987) 247. 4) Pare E. et al. Phys. Lett. **B242** (1990) 531. 5) Arata N. Nucl. Phys. **B211** (1983) 189. 6) Ohsawa A. Prog. Theor. Phys. **92** (1994) 1005. 7) Kafka T. et al. Phys. Rev. **D10** (1974) 3579. 8) Ohsawa A. and Sawayanagi K. Phys. Rev. **D45** (1992) 365. 9) Lattes C.M.G., Fujimoto Y. and Hasegawa S. Phys. Rep. **65** (1980) 152.

A Study of Shower Transition Behaviours Initiated by Hadron-Pb Interaction

M.Tamada

Faculty of Science and Technology,
Kinki University, Osaka, Japan

Abstract

Three-dimensional development of cascade shower in lead initiated by high energy hadron-Pb interaction are calculated by full Monte-Carlo simulation assuming simple geometrical model for hadron-nucleus interactions and also taking account excat geometrical structure of Pamir thick lead chamber. It is shown that fluctuations in shower development is very large but the extroardinary long penetrating showers observed in the experiment can not be explained by simple fluctuations of shower development initiated by ordinary hadron-Pb interactions.

1. Introduction

In Chacaltaya and Pamir coollaboration experiments it has been reported[1] that there exist exotic pheonomena called "Centauro species" in very high energy cosmic-ray nuclear interaction of energy larger than 10^{15} eV. The common characteristics of those exotic phenomena are absence of pions among produced secondary particles and large p_t of produced partcles. Although nature of those partcles is still unknown, there is an argumemnt that those particles are something new different from ordinary hadrons because there found exotic shower-cluster called "mini-cluster" in those hadron interactions and also collision mean free path of those partcles is found to be shorter than that of ordinary hadons. In recent work of Pamir and Chacaltaya collaborations[2], attenuation mean free path of high energy hadrons in super-families of visible energy sum $\Sigma E(\gamma) \geq 700$ TeV observed in thick lead chamber is measured and is found again to be considerably smaller than that of ordinary hadrons. Extraordinary characteristics of those hadrons are also seen in their shower transition behaviours[3]. Some of those hadron-induced cascade showers penetrate almost whole thickness of the chamber without considerable attenuation. Typical examples of shower transition of those are shown in Fig.1. Those extraordinary characteristics can be considered to be related to short collision mean free path of hadrons. That is, suuccessive intarections happen so frequently, because of the short collision mean free path, that electromagnetic cascades initiated by the successive interactions begin to develop before the attenuation of the preceding electromagnetic cascades. In the present paper we study nuclear and electromagnetic cascade development in lead initiated by hadron-Pb interactions assuming simple geometrical model for hadron-nucleus interactions, and compare with experimental results.

2. Nuclear and electromagnetic cascade in thick lead chamber initiated by hadron-Pb interaction

Hadron-nucleus interaction

Here we use simple geometrical model for hadron-nucleus interaction. Some details of the model are described in the separate paper[4]. The number of target mucleons that would interact with projectile hadron is sampled from Poisson distribution with an average depending on impact parameter of collision. Each sub-interaction is treated as a usual hadron-nucleon interaction and phenomenological UA5 algorithm[5] is used for it. Here we assume, for simplicity, all produced particles are pions.

Nuclear cascade inside the chamber

We calculate development of nuclear cascade in the lead chamber under the assumptions that ;

1) energy spectrum of hadrons arriving upon the chamber is power-type of $I(\geq E) \propto E^{-\beta}$ with integral power index $\beta=2.0$,

2) azimuthal distribution of arriving hadrons is $I(<\cos\theta) \propto (\cos\theta)^{-8}$,

3) total thickness of the chamber, T_{eff}, is 60 cmPb.

300 protons of $E \geq 100$ TeV are sampled from the above energy spectrum, and nuclear cascades initiated from interaction of those are traced down until energy of all hadrons, both projectile and produced, becomes less than 0.2 TeV or arriving at the bottom of the chamber.

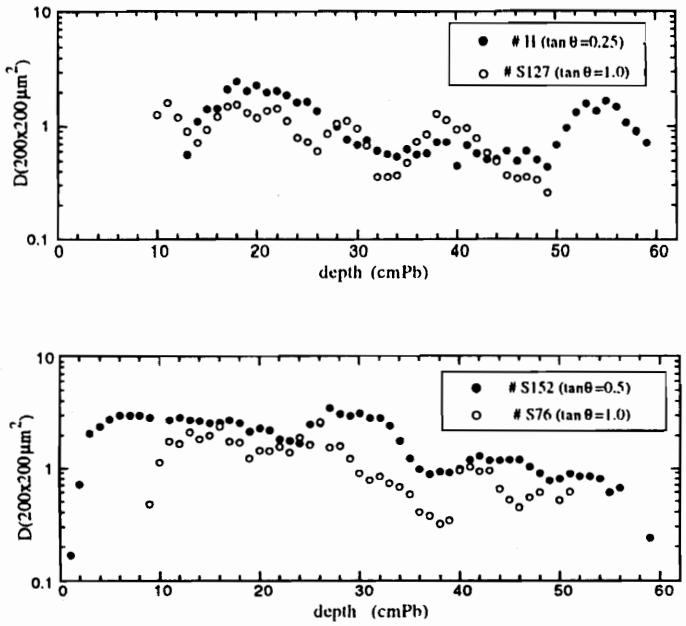

Fig.1 Examples of shower transition on spot darkness found in Pamir thick lead chambers[2,3].

Electromagnetic cascade inside chamber

Among produced hadrons, neutral pions decay into gamma-rays. Further three-dimensional electromagnetic cascade development initiated from those gamma-rays of energy larger than 0.02 TeV is calculated also by Monte-Carlo method taking into account exact structure of Pamir thick lead chamber, 60 layers of 1 cm thck lead plate. Monte Carlo code of electromagnetic shower development inside the chamber, here we used, were completed by T.Shibata[6]. There, Landau-Pomeranchuk effect to the cross section for high energy particles, effects of ionization loss and Compton scattering for low energy particles are also taken into considerations. Electrons and photons are traced down until their energy becomes 1 MeV. After calculations of electromagnetic cascade development of all gamma-rays of $E\gamma \geq 0.02$ TeV, we obtain electron number in a ring of width 6.25 μm at every 6.25 μm from incident hadron direction under every 1 cm thick of lead in whole the depth of the chamber. Electron number density, ρ, is transformed into darkness, D, of X-ray film, measured by 200 x 200 μm^2 slit, by using characteristic relation of the Russian RT6-type X-ray film,

$$D = D_0 (1 - \exp(-\alpha\rho))$$

with $D_0=4.0$ and $\alpha=1.48/\mu m^2$, and finally we obtain shower transition on spot darkness throughout the chamber.

3. Shower transition curve initiated from proton-Pb interaction

Fig.2 shows several examples of hadron-induced shower transition curve on spot darkness obtained by the above calculations. As is seen in the figure, general charateristics of those shower transitions are

1) they have wave-like structure with multiple-peak,

2) the first peak gives shower maximum in almost all events,

3) distance between neighbouring peaks is 10 - 20 cmPb.

Some of the high energy events have very long tail after the first peak of shower ttransition, but attenuation rate seems much faster than that of experimentally observed shower transition shown in Fig.1

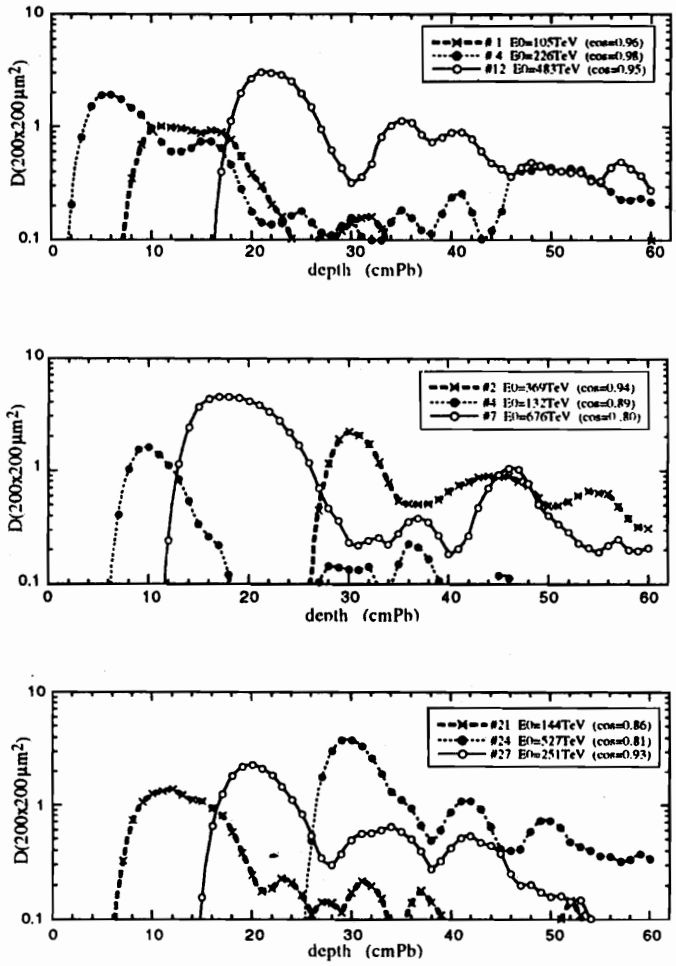

Fig.2 Examples of simulated shower transition on spot darkness.

Relationship between released energy sum and sum of spot darkness

In Fig.3 we show a correlation diagram on sum of energy, $\Sigma E\gamma$, released in form of gamma-rays in hadron-Pb interactions and sum of spot darkness with $D_i \geq 0.3$, measured by $200x200\mu m^2$ slit, $\Sigma D_i(D_i \geq 0.3)$, in its shower transition. Standard photometric measurement on spot darkness in the experiment is limited to spot darkness D=3.5, then here we put D_i=3.5 if spot darkness D_i gives larger than 3.5 in simulation calculations. As is expected we can see ΣD is proportional to $\Sigma E\gamma$, dotted line in the figure represents a relation $\Sigma D \propto \Sigma E\gamma$, except for those which made interaction at the bottom of the chamber and cascade shower does not yet fully develop, situated far from the main stream in the figure.

Width of shower transition.

Here we define width of shower transition curve, D_{width}, as number of successive layers which have spot darkness larger than $0.5 \cdot D_{max}$, where D_{max} is spot darkness at shower maximum in the shower transition on spot darkness. Fig.4 shows correlation diagram on D_{width}, width of shower transition define above, and $\Sigma D_i(D_i \geq 0.3)$, sum of spot darkness with $D_i \geq 0.3$ in those shower transition. Here also we put D_{max}=3.5 if Dmax gives larger than 3.5 in simulation calculations. For inclined showers, D_{width} is also corrected for zenith angle θ, that is, $D_{width} = D_{width}/\cos\theta$. It is seen in simulated data that Dwidth becomes large when ΣD is large, that is released energy, $\Sigma E\gamma$, is large. In Fig.5 we show a correlation digram on

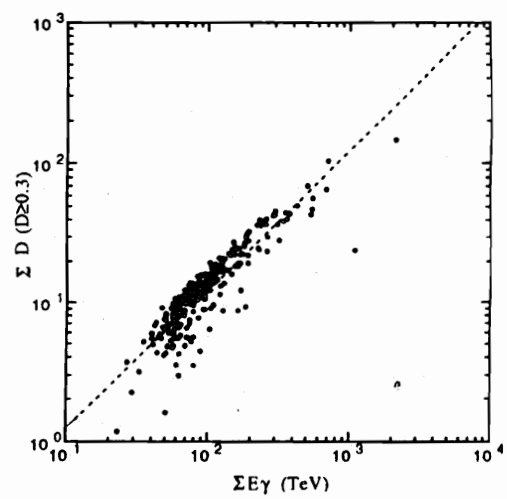

Fig.3 Correlation diagram on sum of spot darkness, $\Sigma D(D \geq 0.3)$, and sum of energy released into gamma-rays in hadron-Pb interactions.

D_{max} and D_{width} for the events which have $\Sigma D_i(D_i \geq 0.3) \leq 55$, correspond to $\Sigma E\gamma \leq \sim 400$ TeV as is seen in Fig.3. We can see in those figures, there exist events in the experimental data which have extraordinary large value of D_{width}, say $D_{width} > \sim 15$-20, even though released energy sum and D_{max} are not so high.

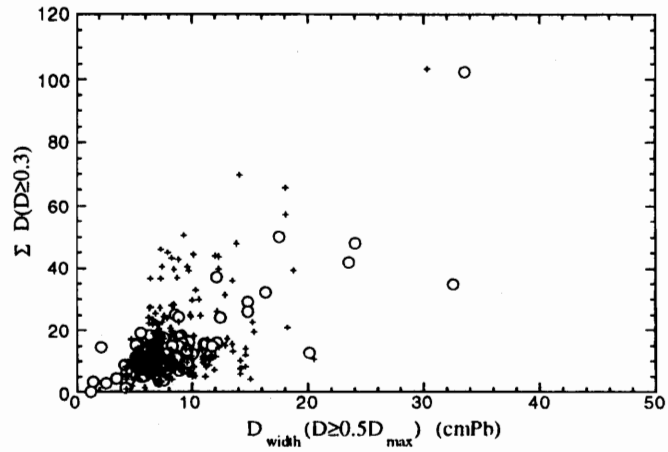

Fig.4 Correlation diagram on sum of spot darkness, $\Sigma D(\geq 0.3)$, and width of shower transition, $D_{width}(D \geq 0.5D_{max})$. (O) for 128 experimental data and (+) for 287 simulated data.

4. Sumary and Discussions

We have shown there exist events which show extraordinary large penetrating shower transition on spot darkness, far beyond fluctuation expected from ordinary hadron-nucleus interactions. Darkness of shower maximum in those showers is not so large but showers continue very deep in the chamber. One of the possible interpretations is to assume short collision mean free path of incident and/or produced particles. In this case, succeeding electromagnetic cascades develop before preceding cascades attenuate and shower transition curve of those showers is expected to be very penetrative without considerable attenuation.

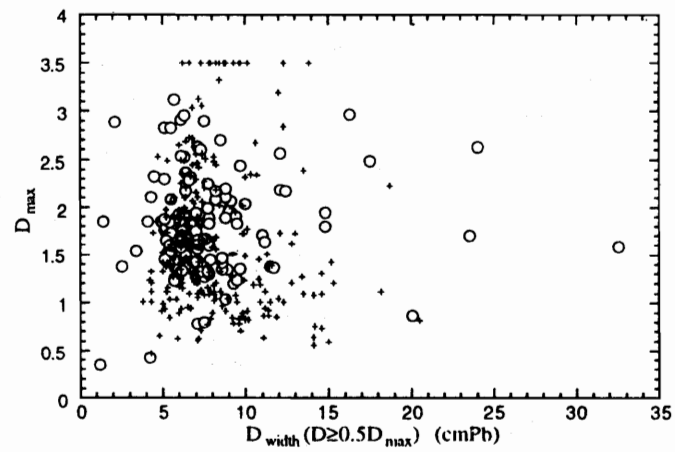

Fig.5 Correlation diagram on spot darkness at shower maximum, D_{max}, and width of shower transition, $D_{width}(D \geq 0.5D_{max})$ for the events with $\Sigma D \leq 55$. (O) for 127 experimental data and (+) for 282 simulated data.

References

[1] Chacaltaya and Pamir Collaboration (L.T.Baradzei et al.) : Nucl.Phys.B370 (1992) 365
C.M.G.Lattes et al. : Phys. Rep.65 (1980) 151

[2] Chacaltaya and Pamir Collaboration (T.Arisawa et al.) : Nucl. Phys.B424 (1994) 241

[3] Chacaltaya and Pamir Collaboration (G.F.Fedorova et al.) : Proc. 24th Int. Cosmic-Ray Conf. Rome, HE1 in this volume

[4] M.Tamada : Proc. 24th Int. Cosmic-Ray Conf. Rome, HE1 in this volume

[5] UA5 collaboration (G.L.Alner et al.) : Nucl.Phys.B291(1987) 445

[6] M.Okamoto and T.Shibata : Nucl. Instr. and Meth. A257(1987) 155.

Attenuation Mean Free Path of High Energy Hadrons in Lead

M.Tamada

Faculty of Science and Technology, Kinki University, Osaka, Japan

Abstract

Attenuation mean free path, λ_{att}, of nucleons and pions in thick lead chambers is calculated assuming simple geometrical model for hadron-nucleus interactions and also taking experimental procedure into considerations. It is shown that λ_{att} of hadrons in high-energy families observed by Pamir and Chacaltaya collaboration experiment is much smaller than that of ordinary hadrons.

1. Introduction

In recent work of Pamir and Chacaltaya collaborations[1], it is argued that the attenuation mean free path of hadrons in super-families of visible energy sum $\Sigma E(\gamma) \geq 700$ TeV is considerably smaller than that of ordinary hadrons. Relationship between attenuation mean free path and collision mean free path is not straightforward, it depends on energy spectrum of incident hadrons, inelasticity distribution on hadron-nucleus interaction, detecting method of hadrons and so on. In the present paper we estimate attenuation mean free path for ordinary hadrons in the thick lead chambers assuming simple geometrical model for hadron-nucleus interactions, and compare with experimental results.

2. Geometrical model of hadron-nucleus interactions

Inelastic cross-section for hadron-nucleus interaction.

We assume projectile hadron moves through a nucleus on a straight line, interacting with encountered target nucleons as it pass through, as is usually assumed in models of hadron-nucleus collisions[2]. The probability to make ν collisions at an impact parameter b, $P_\nu(b)$, in $-\infty < z < \infty$ is given by

$$P_\nu(b) = \frac{1}{\nu!}(\sigma T(b))^\nu \exp(-\sigma T(b)) \quad , \quad T(b) \equiv \int_{-\infty}^{\infty} \rho(b,z)\, dz \,. \tag{1}$$

The inelastic cross-section for hadron-nucleus interaction is then given by

$$\sigma_{h\text{-}A}^{inel} = \sum_{\nu=1}^{A} P_\nu \cong 2\pi \int_0^\infty b\, db\, [1 - \exp(-\sigma T(b))] \tag{2}$$

where A is atomic number of target nucleus. In the following we use Wood-Saxon form for nuclear density, that is,

$$\rho(r) = \frac{\rho_0}{1 + \exp(\frac{r - r_0}{a})} \quad , \quad \rho_0 = \frac{3A}{4\pi r_0^3(1 + \frac{\pi^2 a^2}{r_0^2})} \tag{3}$$

with parameters $r_0 = 1.19\, A^{1/3} - 1.61\, A^{-1/3}$ fm and $a = 0.54$ fm [2,3].

Energy dependence of inelastic cross-section, σ, for elementary hadron-nucleon collision is drawn from the one given by Hillas[4]. Inelastic cross-section for nucleon-Pb and for pion-Pb interaction is calculated by the eq.(2), and the results are shown in Fig.1.

Inelastic hadron-nucleus interaction.

The number of target mucleons that would interact with projectile hadron is sampled from the Poisson distribution given by eq.(1). Here the projectile hadron is assumed to impinge on target

nucleus at a random impact parameter and to be always in "hadron state". Each sub-interaction can be treated as a usual hadron-nucleon interaction and phenomenological UA5 algorithm[5] is used for it. We assume here no internuclear cascade for produced particles. Our algorithm for inelastic hadron-nucleus interaction is summarized as follows;

1) sample an impact parameter b from random distribution,

2) sample number of sub-collisions ν from eq.(1),

3) generate secondary particles by using UA5 algorithm for each sub-interaction. The ratio of single-diffraction, both projectile and target, to non-single-diffraction process in each sub-interaction is assumed to be 0.19. Here we assume, for simplicity, all produced particles are pions.

4) repeat the process 3) ν times or until projectile hadron energy becomes below 10 GeV.

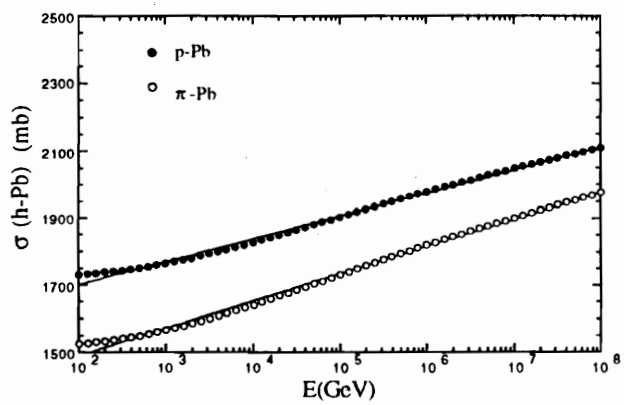

Fig.1 Energy dependence of cross-section σ(h-Pb)

3. Nuclear cascade in thick lead chamber

We calculate development of nuclear cascade in the lead chamber under the assumptions that ;

1) energy spectrum of hadrons arriving upon the chamber is power-type of $I(\geq E) \propto E^{-\beta}$ with integral power index β, β=2.0 for single-arrived hadrons and β=1.3 for hadrons in families.

2) total thickness of the chamber, T_{eff}, is 100 cmPb.

100,000 protons and pions, respectively, of $E \geq 10$ TeV are sampled from the above energy spectrum, and nuclear cascades initiated from interaction of those are traced down until energy of all particles, both projectile and produced, becomes less than E_{cut} or arriving at the bottom of the chamber. During calculations of nuclear cascades, distance of interaction points measured from the top of the chamber and released energy sum, $E(\gamma) \equiv \Sigma E_{\pi^0}$, in form of π^0-mesons in each interaction are recorded if $E(\gamma)$ is larger than E_{cut}.

4. Distribution of interaction points (ΔT-distribution)

In the experiment, depth of interaction points of hadrons are defined by ΔT, horizontal shift of experimental transition curve with respect to the "best-fitted" theoretical curve around shower-maximum region. In hadron-induced showers, we often observe multi-bump structure in its shower transition. If the distance between two bumps is not large, we can identify those two bumps are due to successive interaction of single hadron and the above ΔT determination is applied for the maximum bump. However, if the distance between two bumps is very large, we often misidentify those two bumps as coming from two different hadrons, especially in case of the study of single-arrived hadrons. Then we construct distribution of interaction points, i.e., ΔT-distribution , in simulation calculations for the following two cases;

A) If there are several points of interaction which give $E(\gamma) \geq E_{cut}$ in single nuclear cascade, we define ΔT as a depth of the point which has maximum $E(\gamma)$ among those interaction points, and

B) all interaction points which give $E(\gamma) \geq E_{cut}$ in single nuclear cascade are taken into considerations for measures of ΔT.

Attenuation mean free path of single-arrived hadrons.

Fig.2 shows simulated depth distribution of interaction points which give rise to $E(\gamma) \geq 6.3$ TeVfor the case of proton incidence with energy spectrum $I(\geq E) \propto E^{-2}$. In the figure, (Δ) stands for the case A and (O) for the case B of ΔT determination. Straight lines in the figures are best-fitted ones in the interval of $20 \leq \Delta T \leq 170$ c.u. and we can estimate attenuation mean free path for case A [for case B] as,

204.4 ± 4.0 g/cm^2 [220.4 ± 4.4 g/cm^2] protons
224.3 ± 3.8 g/cm^2 [239.6 ± 3.6 g/cm^2] pions

The difference between case A and case B, and also between proton incidence and pion incidence is not so large. The experimental results[6] for single-arrived hadrons is also shown by closed circles in the figures for the comparison. The experimental procedure to get ΔT-distribution is same neither to the case A nor to the case B, but is just a mixture of both cases. The single-arrived hadrons are considered to be mainly protons, and the results then could be compared with intermediate value of calculations for case A and case B of proton incidence. Although the experimental distribution shows not simple exponential behavior, the attenuation mean free path is estimated in the range $20 \leq \Delta T \leq 80$ c.u. to be $\lambda_{att} = 209 \pm 17$ g/cm^2[6]. Thus the experimental distribution of ΔT for single arrived hadrons agrees well to the simulated ones in the region of $\Delta T < 100$ c.u.. Beyond $\Delta T \approx 100$ c.u., however, experimental data shows less attenuation rate.

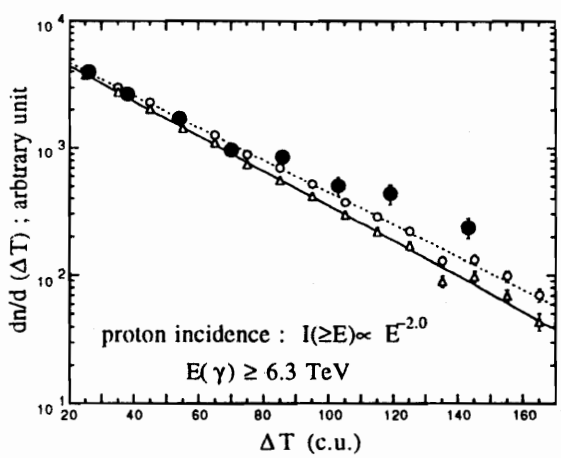

Fig.2 ΔT distribuion for single-arrived hadrons.

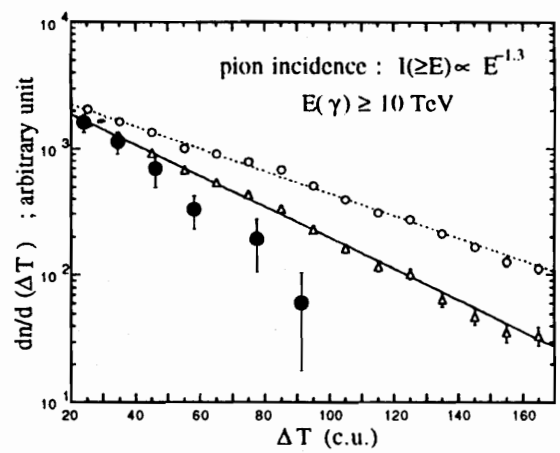

Fig.3 ΔT distribuion for hadrons in families.

Attenuation mean free path of hadrons in super-families.

Fig.3 shows simulated depth distribution of interaction points which give rise to $E(\gamma) \geq 10$ TeV for the case of pion incidence with energy spectrum $I(\geq E) \propto E^{-1.3}$. Straight lines in the figures show best-fitted ones in the interval $20 \leq \Delta T \leq 170$ c.u. and attenuation mean free path for case A [for case B] is obtained as,

207.8 ± 7.2 g/cm^2 [275.6 ± 7.3 g/cm^2] protons
229.8 ± 7.4 g/cm^2 [316.9 ± 13.7 g/cm^2] pions

In usual type of interaction, the produced secondary hadrons are mainly pions. Then hadrons in families are expected to be mainly pions and we can compare experimentally observed attenuation mean free path with that of pion incidence. In the case of hadrons in families, tracing of shower spot down into deeper layer is much easier than in the case of single-arrived hadrons, because we can find many reference shower spot even in deeper layers. Then the case A is more

probable for the comparison for hadrons in families. In Fig.3 also shown are the experimental distribution on ΔT of hadrons in 17 super-families of $\Sigma E(\gamma) \geq 700$ TeV[1]. The experimental value on λ_{att} estimated by using 142 high energy hadrons of visible energy $E(\gamma) \geq 10$ TeV in those super-families is known to be $\lambda_{att} = 176 \pm 48$ g/cm^2 by least square method in the interval of $10 \leq \Delta T \leq 100$ c.u., and $\lambda_{att} = 170\ ^{+47}_{-26}$ g/cm^2 by maximum likelihood method[1]. Those values are considerably smaller than that of case A of the simulated value, 229.0 ± 7.3 g/cm^2, of pion incidence. Even when we assume secondary hadrons in super-families are not pions but mostly nucleons, the experimentally observed λ_{att} is still smaller than that of nucleon incidence, $\lambda_{att} = 207.8 \pm 7.2$ g/cm^2. In Table 1 we show summary of the above argument. In the table also given are λ_{att} for the case where we assume 20% of π-Pb interactions have charge exchange process. As is seen in the table, no considerable affects of charge exchange process are seen.

Table 1. Summary of attenuation mean free path and collision mean free path.

integral power index	visible energy of hadrons	procedure	λ_{att} (g/cm^2) nucleon	pion	experiment [1,6]
β=2.0	$E(\gamma) \geq 6.3$ TeV	A	204.4 ± 4.0 (206.3 ± 3.7)	224.3 ± 3.8 (221.0 ± 5.8)	209 ± 17 *
		B	220.4 ± 4.4 (222.4 ± 4.0)	239.6 ± 3.6 (236.4 ± 5.7)	
β=1.3	$E(\gamma) \geq 10$ TeV	A	207.8 ± 7.2 (204.3 ± 7.4)	229.8 ± 7.4 (221.1 ± 5.8)	176 ± 48 $[170\ ^{+47}_{-26}]$
		B	275.6 ± 7.3 (284.4 ± 9.2)	316.9 ± 13.7 (292.8 ± 7.6)	
	$E(\gamma) \geq 20$ TeV	A	202.2 ± 4.3 (198.1 ± 7.6)	224.1 ± 6.3 (218.1 ± 8.0)	146 ± 40 $[137\ ^{+57}_{-26}]$
		B	311.1 ± 6.7 (273.3 ± 11.0)	308.8 ± 7.8 (281.6 ± 10.7)	
λ_{coll} (g/cm^2)			190 - 180	210 - 200	

Figures in ( ) are for the case where 20 % of π-Pb interactions are asuumed to be charge exchange process.
* : estimated by least square method in the interval $20 \leq \Delta T \leq 80$ c.u..
Figures in [ ] are estimated by maximum likelihood method.

5. Summary and Discussions

We have studied expected attenuation mean free path, λ_{att}, of pions and nucleons in thick lead chamber by constructing simple geometrical model for hadron-nucleus interactions. λ_{att} of single-arrived hadrons, which are considered to be mostly protons, observed in the Pamir and Chacaltaya collaboration experiment well agrees with calculations for proton inicidence. For hadrons in high-energy families, however, calculations fail to explain the experimentally observed short attenuation mean free path. It seems to indicate the existence of new hadronic phenomena in high-energy cosmic-ray nuclear interactions.

References

[1] Chacaltaya and Pamir Collaboration (T.Arisawa et al.) : Nucl. Phys.B424 (1994) 241
[2] K.Werner : Phys.Rev.D39(1987) 780
[3] N.Suzuki : Theor. Phys. 67(1982) 571, Nucl. Phys.A403(1983) 553.
[4] A.H.Hillas : Proc. 16th Int. Cosmic-Ray Conf. Kyoto (Inst for Cosmic Ray Research, Univ. of Tokyo, 1979) Vol.6, p.13
[5] UA5 collaboration (G.L.Alner et al.) : Nucl.Phys.B291(1987) 445
[6] Pamir collaboration : Proc. Int. Sym. on Cosmic Ray and Particle Physics, Tokyo(1984) p.426

Wavelet Analysis of High Multiplicity Events

Naomichi Suzuki, Minoru Biyajima[1] and Akinori Ohsawa[2]
Matsusho Gakuen Junior College, Matsumoto 390-12
[1] Department of Physics, Shinshu University, Matsumoto 390
[2] Institute for Cosmic Ray Research,University of Tokyo,Tanashi 188

Abstract

Pseudo-rapidity distributions of two high multiplicity events Ca-C and Si-AgBr observed by the JACEE are analysed by the wavelet transform. Wavelet spectra of those events are calculated and compared with the simulation calculations with Poisson random numbers, uniformly random numbers and a p-model. The wavelet spectrum of Ca-C resembles to that simulated with the uniform random numbers, but that of Si-AgBr is not reproduced by any of the simulation calculations.

In high energy ncleus-nucleus collisions, studies of number density fluctuations in the rapidity space is expected to reveal new features of multiparticle production mechanisms. In this paper, pseudo-rapidity η distributions of the two JACEE events, Ca-C and Si-AgBr[1] are analysed by the wavelet transform [2]. Any function (data) can be expanded by self-similar wavepackets in this scheme. Therefore characteristics of local fluctuations can be extracted from the data.

Orthonormal wavelets are constructed from dilation and translation of a scaling function $\phi(x)$. It is constructed by an iteration equation,

$$\phi_i(x) = \sum_{k=0}^{N-1} c_k \phi_{i-1}(2x-k) \quad i = 1, 2, \cdots, \tag{1}$$

from a primary scaling function, whcih is defined as $\phi_0(x) = 1$ for $0 \leq x < 1$, and otherwise $\phi_0(x) = 0$. In Eq.(1), N is a even number, and c_k $(k = 0, 1, \cdots, N-1)$ are constants. The iteration is continued until $\phi_i(x)$ becomes indistinguishable from $\phi_{i-1}(x)$, and $\phi(x)$ is defined by this $\phi_i(x)$. The mother wavelet $W(x)$ is given by

$$W(x) = \sum_{k=0}^{N-1} (-1)^{k+1} c_{N-1-k}\, \phi(2x-k), \tag{2}$$

and the j-th level wavelet $(j = 0, 1, \cdots)$ is defined as

$$\psi_{j,k}(x) = 2^{\frac{j}{2}} W(2^j x - k), \qquad k = 0, 1, \cdots, 2^j - 1. \tag{3}$$

Then any function $f(x)$ (defined for $0 \leq x < 1$) can be expanded by the wavelets as

$$f(x) = a_0\,\phi(x) + \sum_{j=0}^{\infty}\sum_{k=0}^{2^j-1} \alpha_{j,k}\,\phi_{j,k}(x).$$

If $N = 4$, coefficients $c_k\,(k = 0, 1, \cdots, N-1)$ are given by

$$c_0 = \frac{1+\sqrt{3}}{4}, \quad c_1 = \frac{3+\sqrt{3}}{4}, \quad c_2 = \frac{3-\sqrt{3}}{4}, \quad c_3 = \frac{1-\sqrt{3}}{4}.$$

Let $f(x)$ be given by descrete value, $f_i = f(\Delta/2 + \Delta \cdot (i-1))$ $(i = 1, 2, \cdots, 2^r)$, where $\Delta \cdot 2^r = 1$. $f(x)$ is assumed to be periodic outside the defined region $0 \leq x < 1$. By the use of column matrices,

$$F = \begin{pmatrix} f_1 \\ \cdots \\ f_{2^r} \end{pmatrix}, \qquad A_j = \begin{pmatrix} \alpha_{j,0} \\ \cdots \\ \alpha_{j,2^j-1} \end{pmatrix}, \quad j = 0, 1, \cdots, r-1,$$

the wavelet transform is given by

$$\begin{aligned} a_0 &= 2^{-\frac{r}{2}} L_1 L_2 \cdots L_r F, \\ A_{j-1} &= 2^{-\frac{r}{2}} H_j L_{j+1} \cdots L_r F, \quad j = 1, 2, \cdots, r-1, \\ A_{r-1} &= 2^{-\frac{r}{2}} H_r F. \end{aligned} \tag{4}$$

L_j and H_j are $2^{j-1} \times 2^j$ matrices. The i-th row of L_j is expressed as,

$$\begin{aligned} &\begin{pmatrix} 0 & \cdots & 0 & l_{2(i-1)+1} & \cdots & l_{2(i-1)+k} & \cdots & l_{2(i-1)+N} & 0 & \cdots & 0 \end{pmatrix} \\ &= \frac{1}{\sqrt{2}} \begin{pmatrix} 0 & \cdots & 0 & c_0 & \cdots & c_k & \cdots & c_{N-1} & 0 & \cdots & 0 \end{pmatrix}. \end{aligned}$$

If $2(i-1) + k > 2^j$, element $l_{2(i-1)+k}$ is added to the $(2(i-1) + k - 2^j)$-th element in each row. Matrix H_j is obtained if c_k $(k = 0, 1, \cdots, N-1)$ in L_j is replaced by $(-1)^{k+1} c_{N-1-k}$.

The j-th level wavelet spectra E_j $(j = 0, 1, \cdots, r-1)$ is defined by

$$E_j = \sum_{k=0}^{2^j-1} \alpha_{j,k}^2 = {}^t A_j A_j, \qquad j = 0, 1, \cdots, r-1. \tag{5}$$

The background distributions [3],

$$f_0(\eta) = A\left[(1 - e^{-Y-\eta})(1 - e^{-y+\eta})\right]^B, \quad -Y \leq \eta \leq Y, \tag{6}$$

$$A = 81,\ B = 5.4, Y = 7.0 \qquad \text{for Ca} - \text{C},$$

$$A = 184, B = 8.1, Y = 5.5 \qquad \text{for Si} - \text{AgBr}.$$

are subtracted from η distributions of Ca-C and Si-AgBr, respectively. Those η distributions are given with the bin size $\Delta\eta = 0.1$, and data points with $-3.0 \leq \eta < 3.4$ for Ca-C, and $-2.7 \leq \eta < 3.7$ for Si-AgBr (2^6 points) are used in the analysis.

In Fig.1a and 1b, the wavelet spectra E_j ($j = 0, 1, \cdots, 5$) of Ca-C and Si-AgBr are shown, respectively. The full circles show the wavelet spectra of the distributions where backgrounds are subtracted. For the sake of comparison, wavelet spectrum of the raw distribution (without subtraction of the backgrounds) is shown by white circles. The results are different at the 0-th and the first level, but those from j=2 to j=5 are almost the same.

The wavelet spectra E_j ($j = 2, \cdots, 5$) of the distributions, where backgrounds are subtracted, are compared with the following simulation calculations;

(i) Poisson random numbers with the mean μ and the standard deviation $\sigma = \sqrt{\mu}$.

(ii) Uniform random numbers from 0 to a. The mean μ and the standard deviation σ are respectively given as $\mu = a/2$ and $\sigma = \sqrt{3}a/6$

(iii) A p-model[4] with a fraction p_a ($p_b = 1 - p_a$) and an initial 'energy' (or particle number) E_0 in a rapidity interval Δy. E_0 is devided into $p_a E_0$ in one sub-interval of Δy, and $p_b E_0$ in the other one at the first step, as the interval Δy splits into two sub-intervals with equal width. After n steps, the mean μ and the standard deviation σ are given by

$$\mu = \frac{E_0}{2^n}, \quad \sigma = \frac{E_0}{2^n}\sqrt{2^n\left(p_a^2 + q_a^2\right)^n - 1}.$$

Each simulation calculations are done 1000 events. Parameters are adjusted to reproduce the standard deviation of each distribution where background is subtracted, because the mean value has no effect on the wavelet spectrum.

We calculate the wavelet spectra E_j^{sm} ($j = 0, 1, \cdots, 5$) of simulated events and count the number of events within a value of z,

$$z = \sqrt{\sum_{j=2}^{5}(\log_2 E_j - \log_2 E_j^{sm})^2}. \tag{7}$$

The results for Ca-C and Si-AgBr are shown in Table 1. For Ca-C, simulation (ii) have the highest rate within $z < 0.8$ among the three simulation calculations. For Si-AgBr, the highest rate within $z < 0.8$ is obtained with (iii), the p-model. Wavelet spectrum of Ca-C is compared with the average $< E_j^{sm} >$ ($j = 2, \cdots, 5$) of simulation (ii) in Fig.1a. That of Si-AgBr is compared with those with (iii), the p-model in Fig.1b. In Fig.1a and b, middle

dashed line denotes the average $< E_j^{sm} >$ $(j = 0, 1, \cdots, 5)$, upper and lower ones are $< E_j^{sm} > \pm \sigma_j^{sm}$ $(j = 0, 1, \cdots, 5)$, where σ_j^{sm} is the standard deviation of simulated spectra. The wavelet spectrum of Ca-C is well described by $< E_j^{sm} >$ of simulation (ii). That of Si-AgBr is not explained by (iii). It remaines almost inside the region $< E_j^{sm} > \pm \sigma_j^{sm}$, but fluctuates along $< E_j^{sm} >$.

Ca-C	Poisson ($\mu = 7.4$)	Uniform ($a = 9.40$)	p-model ($p_a = 0.22, E_0 = 85.3$)
$z < 0.4$	15	25	6
$z < 0.6$	59	75	21
$z < 0.8$	154	197	41
Si-AgBr	**Poisson ($\mu = 16.2$)**	**Uniform ($a = 14.0$)**	**p-model ($p_a = 0.36, E_0 = 340.8$)**
$z < 0.4$	0	0	4
$z < 0.6$	1	3	22
$z < 0.8$	9	8	73

Table 1

Number of simulated events which satisfy the condition $z < 0.4$, $z < 0.6$, or $z < 0.8$ for Ca-C and Si-AgBr. Each simulation is done 1000 events.

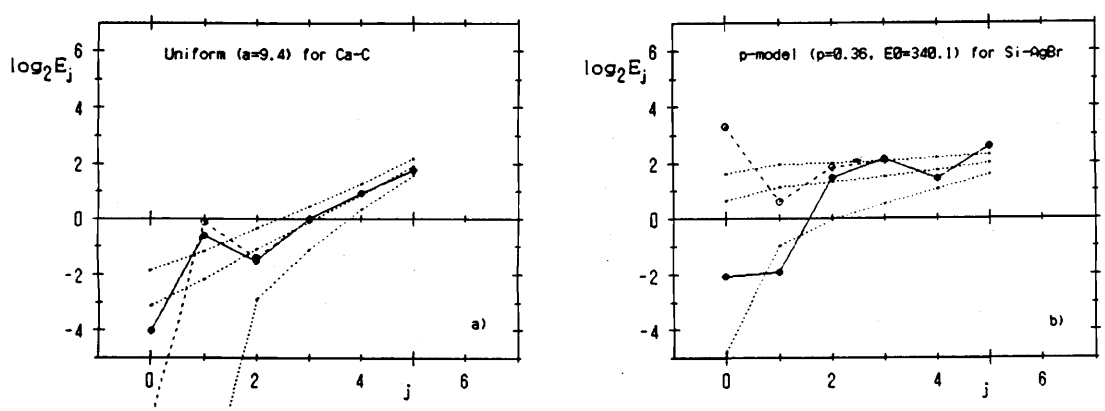

Fig.1 Wavelet spectra of a) Ca-C and b) Si-AgBr. Full circles are calculated from η distributions where backgrounds are subtracted. White circles are from the raw distributions. Dashed lines are obtained from the simulation calculations.

References

[1] T. H. Burnett et al., Phys. Rev. Lett. **50**(1983)2062

[2] I. Daubechies, Comm. Pure and Appl. Math. (1988)909; Ten Lectures on Wavelets, SIAM, Philadelphia, 1992,
D. E. Newland, An Introduction to Random Vibrations, Spectral and Wavelet Analysis, third edition, Longman, Harlow, 1993

[3] F. Takagi, Phys. Rev. Lett. **53**(1984)427

[4] C.Meneveau and K.R.Sreennivasan, Phys. Rev. Lett. **59**(1987)1424

'γ-rays' bundles at the cores of extensive air showers and the primary cosmic ray identification

C.R.A. Augusto[1], $C.E.Navia^1 F.A.Pinto^1$, $S.L.CBarroso^2$, $E.H.Shibuya^2$, M. Luksys[3] $and A.Ohsawa^4$

1 Instituto de Física, Universidade Federal Fluminense, Niterói, RJ, Brasil.

2 Instituto de Física, Universidade Estadual de Campinas, Campinas, SP, Brazil.

3 Departamento de Física, Universidade da Paraiba, 58051-970, PB, Brasil.

4 Institute for Cosmic Ray Research, University of Tokyo, Tokyo 188, Japan

Abstract

We present an useful clue to estimate the energy and chemical composition of the primary cosmic radiation between 10^{14} eV and 10^{17} eV. The method uses various kinds of quantities as measure by an hybrid detector an emulsion chamber in the central part of an EAS (Extensive Air Shower) array at mountain altitude. The procedure permits an analysis on individual events, it gives estimation of the mass and energy of a primary nucleus initiating a shower. We show that EAS size measurement could be complementary to quantities as measured by an emulsion chamber detector to improve the accuracy of the primary cosmic ray identification.

1 INTRODUCTION

The primary cosmic ray composition plays a crucial role in the knowledge of astrophysics particles, because the primary energy spectrum and also the chemical composition are connected with the problems of the origin and propagation of the cosmic particles into and out of the galaxy.

Direct measurements have been done using balloons, air craft and satellites However, these measurements are limited to energies below 10^{14} eV by the low fluxes and the limited exposure time in space or on balloons. A new generation of sophisticated air shower detectors called "hybrid detectors" an emulsion chamber in the central part of an extensive air shower array at mountain altitudes has been developed. The simultaneous observation of high energy γ-rays bundles in emulsion chamber and accompanying EAS in large scale can provide details of the primary cosmic ray composition or in principle distinguish groups of nuclei, with accuracy better than 36%, in the energy region of $10^{15} - 10^{17}$ eV that includes the so called "knee" region in the primary cosmic ray energy spectrum, as well as the characteristic of hadronic interaction in the extremely high energy region, beyond the collider experiments.

In the last years, experimental data in small scale of these hybrid detectors became available by three groups Norikura [1], Tien-Shan [2] and Chacaltaya [3], they have successfully tested the concept. In this context two large scale experiments are planned: the Omega experiment at Chacaltaya (5200 m above sea level) and the Yangbajing experiment at Tibet (5300 m above sea level). The Omega experiment is an up-grade of SYS (Saitama, Yamanashi, San Andres) EAS array and Brazil-Japan emulsion chamber.

In this work an analysis on individual events is carried out. It gives an estimation of the energy and mass number of a primary nucleus, on the basis of a formal argument that permits to construct the joint probability of finding observable quantities with prescribed values. The aim of this report is to examine the accuracy of the method, independent by of the model used to describe the nuclear collision and the posibility of extending the method to practical use in cosmic ray experiments.

2 ANALYSIS ON INDIVIDUAL SHOWERS

The analysis on individual showers carried out in this work, to obtain information on the masses and energies of primary nuclei from observable showers quantities as measured by an hybrid detector was developed on the basis of method reported by Adachi et al. [4]. The method is fully used to get an useful clue to the estimation of the energies of γ-rays and their production heights, from observable quantities of electromagnetic cascade as observed by emulsion chamber.

We make a blow-up of this method to the case of primary nuclei initiating showers, even knowing that stochastic nature of the atmospheric processes smears out identity of the incident primary particle. However, with Monte-Carlo simulation one can derive average quantities and also investigate the fluctuation phenomena.

Let the non-observed quantities: the energy E_o and the mass number A of a primary nucleus starting a shower. The joint probability

$$P(E_o,\ A;\ \sum E_\gamma,\ N_\gamma,\ \sum E_\gamma R_\gamma / \sum E_\gamma)\Delta E_o\, \Delta A, \tag{2.1}$$

of finding E_o and A at prescribed intervals $(E_o + \Delta E_o)$ and $(A + \Delta A)$, for fixed observed quantities $\sum E_\gamma$, N_γ and $\sum E_\gamma R_\gamma / \sum E_\gamma$ can be obtained from figures 1(a), 1(b) and 1(c), mounted via Monte-Carlo method on the basis of a hybrid code composed by a superposition model to describe the number of interacting pairs (wounded nucleons) [5], together with a 'ln s' extrapolation of a model on the basis of accelerator data (UA5 algorithm) [6] to describe the hadronic interaction. They may be presented by the approximation formulas:

$$E_o/E_{th} = (53.16\ A^{0.58})(\sum E_\gamma/E_{th})^{(0.68-0.026\ ln\ A)}, \tag{2.2}$$

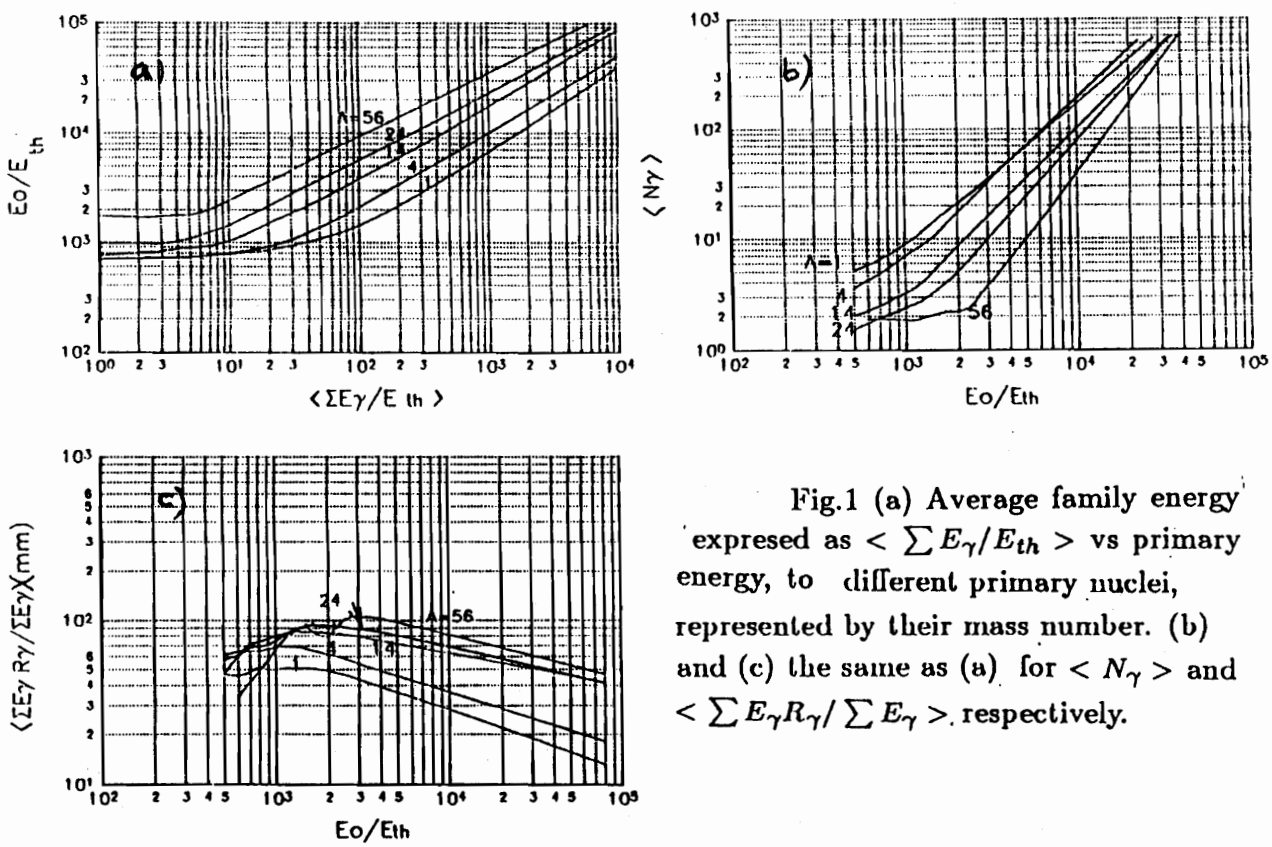

Fig.1 (a) Average family energy expresed as $< \sum E_\gamma/E_{th} >$ vs primary energy, to different primary nuclei, represented by their mass number. (b) and (c) the same as (a) for $< N_\gamma >$ and $< \sum E_\gamma R_\gamma / \sum E_\gamma >$, respectively.

$$E_o/E_{th} = (24.55\ A + 182.6)\ (N_\gamma)^{(0.754-0.056\ ln\ A)}, \tag{2.3}$$

$$E_o/E_{th} = (2.52 \times 10^8\ A^{2.55})(\sum E_\gamma R_\gamma / \sum E_\gamma)^{(-3.04\ A^{0.109})}. \tag{2.4}$$

These parametrizations are valid only by primary energy above 50 TeV and to 540 g/cm^2 of atmospheric depth (Chacaltaya).

For instance at fixed value of $\sum E_\gamma/E_{th}$ we can scan all possible values of A (mass number) in a determined primary energy region, the same procedure can be made using the other two observable quantities.

If the primary nucleus has an energy E_o and a mass number A the joint probability P(E_o,A) will have a relative maximum at E_o and A. Thus, in principle it is possible to estimate the energy and mass of primary nucleus. It can happen that as P(E_o,A) may have several critical points in this case it can be achieved as the maximum point (E_o,A) sufficiently close to E_o estimated as [7] $E_o = 2.0 \times N_e$.

To get the better understanding of the situation the figures 2(a) and 2(b) show the relative probability density $P(E_o, A)d\Delta E_o d\Delta A$ at fixes values of $\sum E_\gamma/E_{th}$, N_γ and $\sum E_\gamma R_\gamma / \sum E_\gamma$ for showers initiated by CNO ($A \sim 14$) and iron respectively

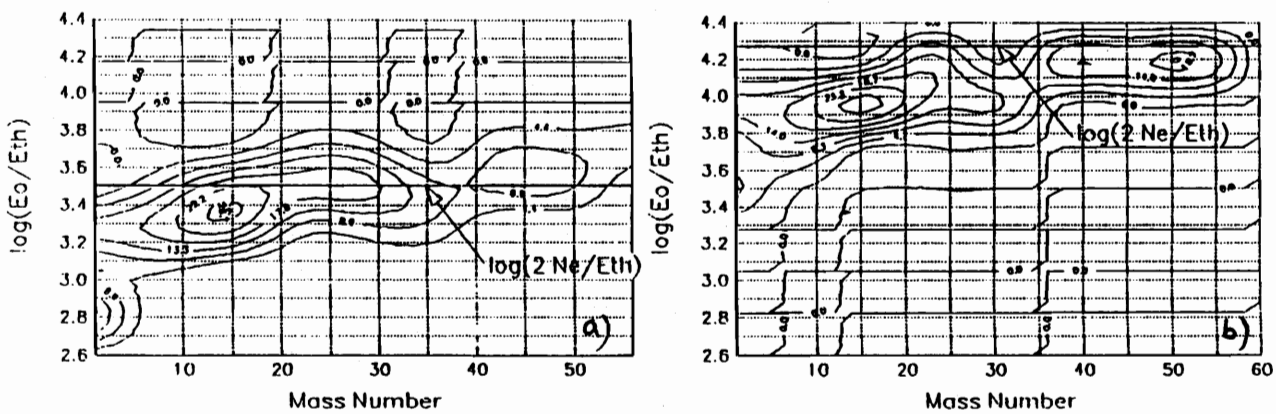

Fig.2 Relative probability density $P(E_o,\ A)\Delta E_o \Delta A$. The analysis on simulated events are shown by: (a) a shower initiated by a primary nucleus with $E_o/E_{th} = 3236$ and $A = 14$; (b) a shower initiated by a primary nucleus with $E_o/E_{th} = 18600$ and $A = 56$. In all the cases the horizontal full line represents the primary energy estimated from EAS size as $E_o = 2.0\ N_e$ (in GeV).

3 ACCURACY IN DETERMINATION OF THE MASS

In order to obtain the accuracy of the method above described a randon selection of 100 simulated events was made, this correspond around 3,000 $m^2 year$ of exposition at Chacaltaya. Distributions of the difference between $A_{estimated}$ and A_{true} are shown in the figures 3(a) and 3(b), for two extreme cases: proton and iron as primary particles respectively. The accuracy test carried out from this method, show to be better than 36% in average, this value includes 12% of events that were discarded because, they presented high ambiguity in their interpretations.

4 CONCLUSIONS

Shower quantities as measured by a combined experimental apparatus can find a breakthrough in the confronting difficulties of EAS and emulsion chamber studies because, the

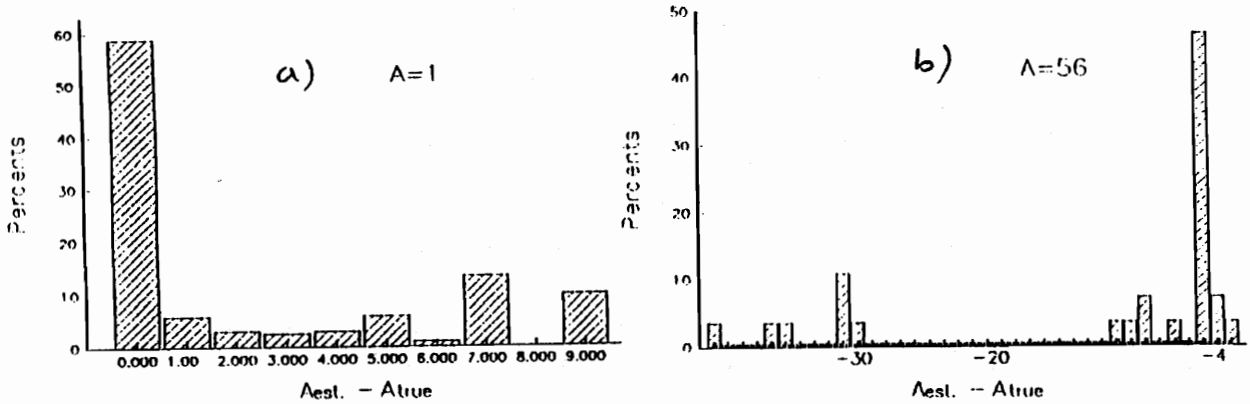

Fig.3 Distribution of the difference between the estimated mass number A_{est} and the true mass number A_{true}. The analysis on simulated events are shown: (a) for proton showers and (b) for irons showers.

correlations between the mean values $< \sum E_\gamma / E_{th} >$, $< N_\gamma >$ and $< \sum E_\gamma R_\gamma / \sum E_\gamma >$ with the primary energy presents a primary mass resolution big enough to permit an analysis on individual event. The knowledge of the primary nucleus energy through the shower size N_e, is crucial to an useful use of the method, because ambiguities in the interpretations of the joint probability function can be avoided.

On the other hand, the accuracy of the method to primary mass identification is better than 36% in average, this value is high enough to resolve the discrepancies on primary composition assumptions or, in other words, confirm a dominant proton or iron composition in the primary cosmic ray particles, in the region of 10^{14} to 10^{17} eV.

[1] T.Saito et al., Astroparticle Physics 1(1993)257.
[2] V.V.Arabkin et al., Proc. 22*nd* Int. Cosmic Ray Conf., Dublin, vol.4,(1991)141,269,273.
[3] N.Kawasumi et al. Proc. 22*nd* Int. Cosmic Ray Conf., Dublin, vol.4,(1991)253.
[4] A. Adachi et al., Supp. of the Prog. of Theo. Phys.,N32(1964)154.
[5] Y.Niihori et al., Phys.Rev. D36(1987)783.
[6] UA5 Collaboration, Nucl. Phys., B (1987)445.
[7] M.Tamada., J.Phys.G: Nucl.Part. Phys. 20 (1994)487

PRODUCTION OF HEAVIER PARTICLES THAN PIONS IN FIRE-BALLS

C.R.Augusto[1], S.L.C.Barroso[2], P.C.Beggio[2], A.O.de Carvalho[2], M.D.O.Marques[2], C.E.Navia[1], R.de Oliveira[2], F.A.Pinto[1], F.R.Revollo[2], E.H.Shibuya[2]
1 Instituto de Física, Universidade Federal Fluminense, 24020-130 Niterói, RJ, Brasil
2 Instituto de Física 'Gleb Wataghin', Universidade Estadual de Campinas, 13083-970 Campinas, SP, Brasil

Abstract

Hadronic interactions detected by upper and lower part of emulsion chamber seems to show production of particles heavier than pions. One of these particles may be eta-meson, observed to be produced by events called Açú by Brasil-Japan Collaboration on Chacaltaya experiments, while Mirim events of smaller multiplicity doesn't show significant production.

Introduction

Brasil-Japan Collaboration (B-J Collaboration) observed some regularity in the phenomena of Multiple Meson Production. The experiments held at Mt.Chacaltaya (5220 m above sea level)-La Paz, Bolivia indicated occurrence of "cluster" of pions decaying isotropically and with high value of transverse momenta. They are called as Mirim, Açú and Guaçú fire-balls. Comparison with accelerator data showed that the correlation between mean pt and multiplicity agrees[1] and so, scaling-law seems to be not valid for higher energy. We did attempts to look for η-meson, because this particle decays also to 2 γ's, same as π^o-meson decay. Both types of data, C-jets and A-jets, i.e. data of interaction in a target layer and in the atmosphere above the chamber are used. Fig. 1a, 1b, 2a and 2b shows histograms of invariant mass of two γ's. They are plotted under following criteria: 1) Selection of events that shows isotropic γ decay in the azimuthal angle; 2) Separation of events in Mirim and Açú according to the analysis of fig. 3a, 3b; 3) Combination of γ pairs after picking up pairs coming from π^o decay. We notice no difference between each pair of figs. 1a, 2a and 1b, 2b, but between figs. 1a, 1b and figs. 2a, 2b it appears a signal over the background estimated by simulation.

On A-jets we tried to recognize pairs of γ's from η-meson decay. For that purpose we used an additional criteria looking for a partner for a γ not coupled to π^o-meson and observed almost far from the center of mass of the event. Some of these highest energy γ's happen to be observed near to another γ's and, if we combine then we obtain an invariant mass close to the η-meson mass. Especially for A-jets events, where the interaction height is not so straightforwardly determined as in C-jets events, it might have room to arguments as superposition of interactions, but these events when analyzed through an algorithm constructed with a convenient combination of energy flow moments it results in a plot of fig. 4, showing that all γ's of the event came mainly from one interaction point and has an isotropic decay.

Fig. 5 shows a transverse momenta of pions superposed with η-mesons plot. The tail part of π^o's coincides with the spectrum of η-mesons and the mean values are $\langle pt_{\pi^o}\rangle = (642\pm43)$ MeV/c and $\langle pt_\eta\rangle = (890\pm134)$ MeV/c.

Discussions and Conclusions

A tail in figs. 1b and 2b shows possible production of particles of higher invariant mass, $M_{\gamma\gamma}$, than π°-meson.

Production of η-mesons seems to be observed in Açú events and no appreciable signal in Mirim events is recognizable.

Mean value of transverse momenta of π°'s is (642±43) MeV/c, but this value is a little higher than previously determined value because it was calculated assuming a single exponential fit.

Mean value of transverse momenta of η-mesons is (890±134) MeV/c , a rather high value, maybe affected by the criterion used for identification of η-meson. Nevertheless, the coincidence between both spectra in the higher values of transverse momenta may be understand as η-meson decaying to γ's, through other decaying channels, mainly $\eta \rightarrow 3\ \pi^{\circ}$'s (branching ratio = 31.9 %) and $\eta \rightarrow \pi^{+}\pi^{-}\pi^{\circ}$ (branching ratio = 23.6 %), comparable with $\eta \rightarrow 2\ \gamma$'s (branching ratio = 38.8 %).

Finally, this analysis showing production of η-meson in Açu fire-balls may be interpreted as a production of heavier particle for higher interaction energy because mean energy of Açú fire-balls is higher than mean energy of Mirim fire-balls.

Acknowledgments

The authors are grateful to B-J Collaboration for the free use of the data. The experiments of B-J Collaboration are supported by FAPESP, CNPq, FINEP in Brasil, by Ministry of Education of Japan and are held in the Mt.Chacaltaya, La Paz-Bolivia with the collaboration of Instituto de Investigaciones Físicas-UMSA.

References

[1] Gaisser T. and Halzen F., Phys.Rev.Lett.54 No.6 (1985),1754

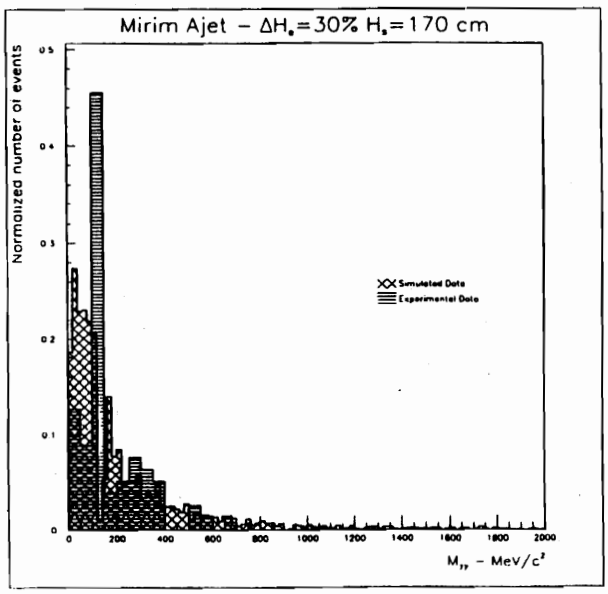

Fig.1a Mirim type

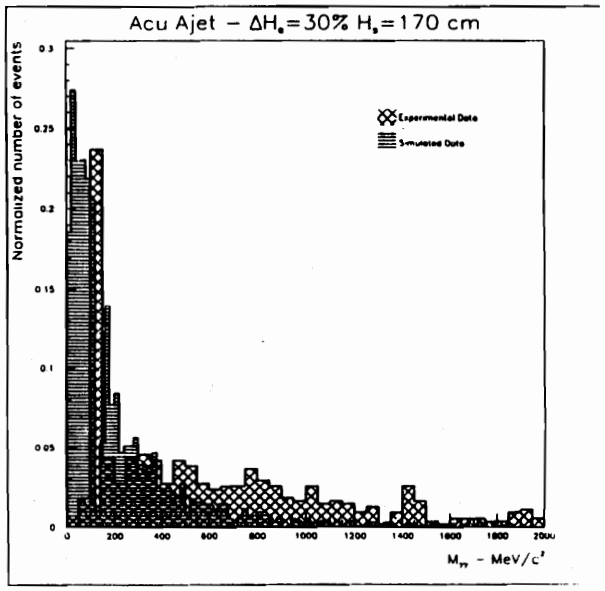

Fig.1b Açú type

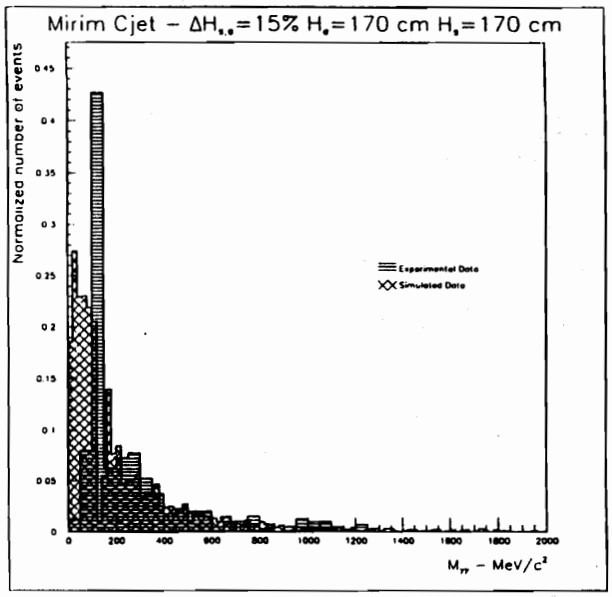

Fig. 2a Mirim type

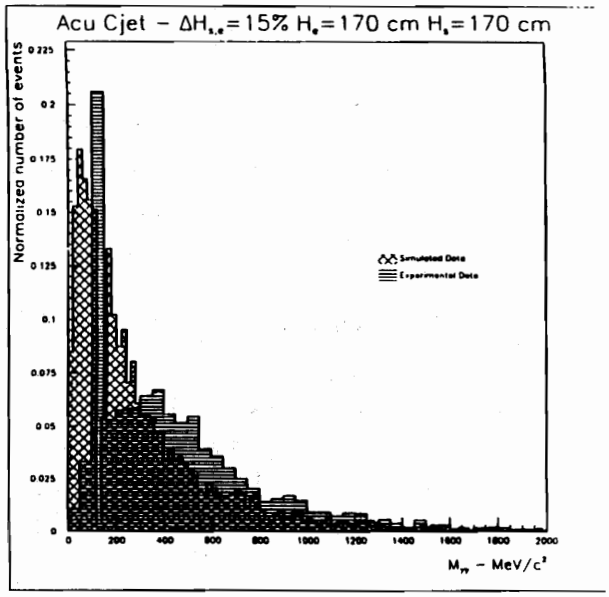

Fig.2b Açú type

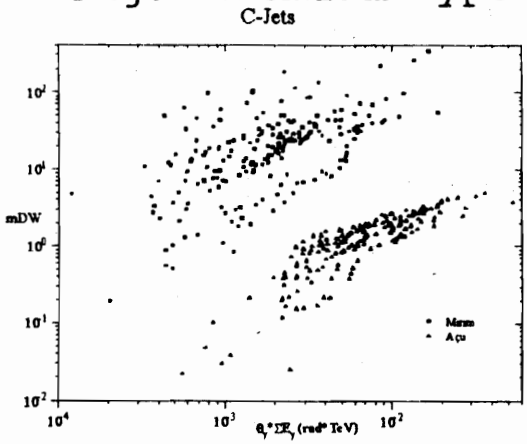

Fig. 3a - mDW applied to isotropic C-Jets

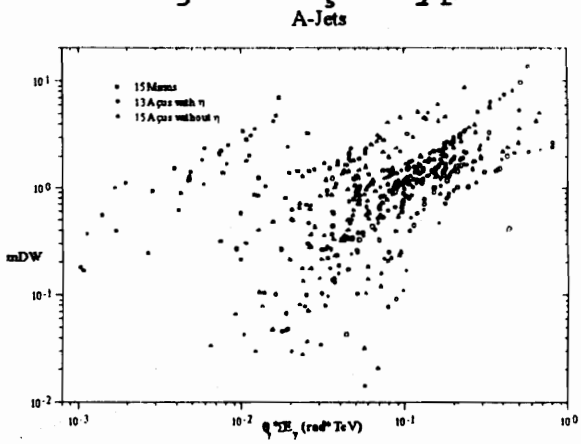

fig. 3b - mDW applied to A-Jets

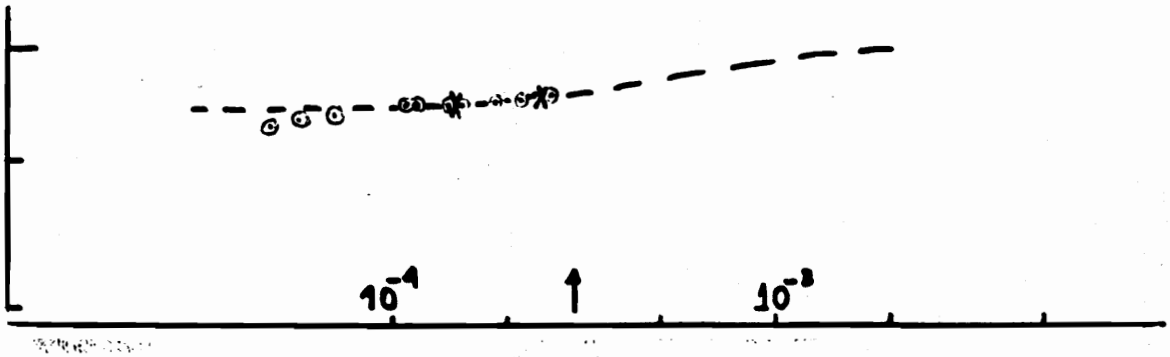

Fig.4 Typical R-plot of A-jet

⊙ γ's from π^0

x γ's " η-meson

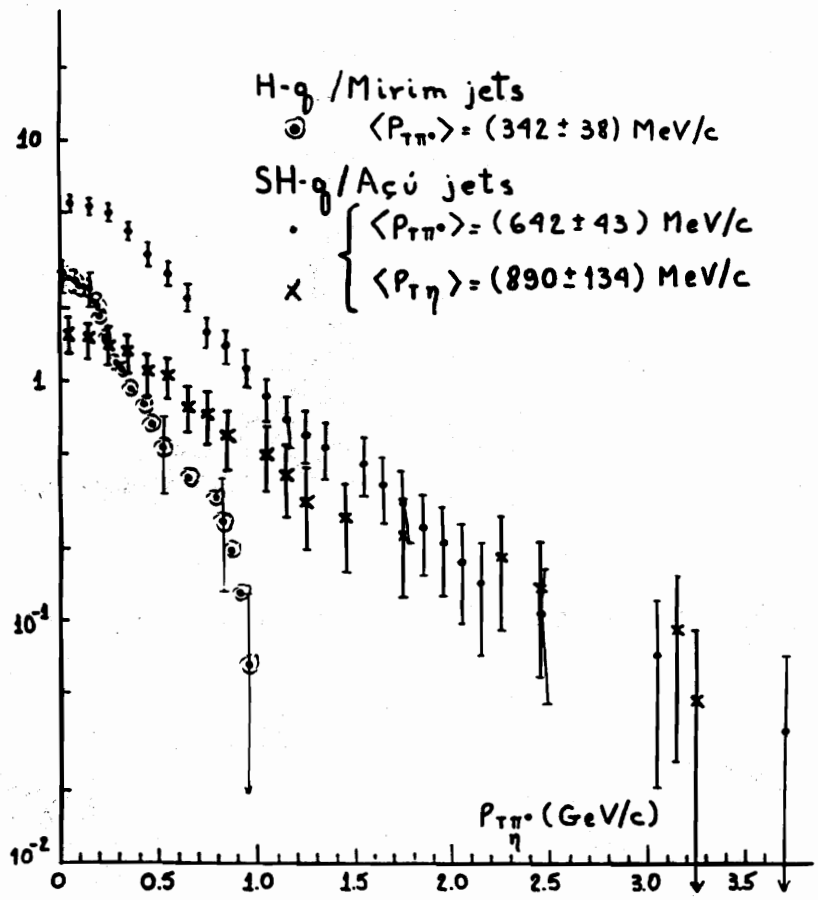

Fig.5 Transverse Momentum of

π^0 or η-meson

Fire-Balls Masses Seen in C-jets

C.R.Augusto[1], S.L.C.Barroso[2], P.C.Beggio[2], A.O.de Carvalho[2], M.Luksys[3], M.D.O.Marques[2], M.J.Menon[2], C.E.Navia[1], R.de Oliveira[2], F.A.Pinto[1], F.R.Revollo[2], E.H.Shibuya[2]

1 Instituto de Física, Universidade Federal Fluminense, 24020-130 Niterói, RJ, Brasil

2 Instituto de Física 'Gleb Wataghin', Universidade Estadual de Campinas, 13083-970 Campinas, SP, Brasil

3 Departamento de Física-CCEN, Universidade Federal da Paraíba, 58059-970 João Pessoa, PB, Brasil

Abstract

Algorithms based in isotropic decay of a fire-ball was applied in C-jets events of Chacaltaya experiments. Through this analysis main result is that the events are well separated in two sets as well established previously by Brasil-Japan Collaboration (B-J Collaboration) on Chacaltaya experiments.

Introduction

Decay products of hadronic interactions obeys isotropy on azimuthal distribution as would be seen applying the so called Duller-Walker plot[1] . B-J Collaboration analyzed C-jets of an experiment (Chamber 15), through a method devēloped by T.Shibata[2] based on isotropic decay of a fire-ball but, this method considered only the first two moments of, ΣE_γ that is, the dependence of energy flow (ΣE_γ) and of transverse momentum flow ($\Sigma E_\gamma \theta_\gamma$) with the emission angle of secondary γ's.

We proceed this method calculating higher order moments and so, it was possible to construct not only $\Sigma E_\gamma \theta_\gamma^2$, $\Sigma E_\gamma \theta_\gamma^3$ but also an algorithm that is the sum of all four moments of ΣE_γ. Explicit expression of this algorithm is,

$$mDW = \frac{1}{4M\Gamma}\left[\Sigma E + \frac{4}{\pi}\Sigma E(\Gamma\theta) + \Sigma E(\Gamma\theta)^2 + \frac{4}{3\pi}\Sigma E(\Gamma\theta)^3\right]$$

where M = invariant mass of γ's cluster (fire-ball),

Γ = Lorentz factor of γ's cluster (fire-ball),

θ = emission angle of γ's and

E = energy of γ's

ploted in fig. 1.

Each of the moments are normalized and so it is necessary to divide by 4 the sum of the four moments and we called the algorithm as modified-"Duller-Walker" plot (mDW), since Duller-Walker method.

This mDW algorithm has an advantage concerning to the traditional Duller-Walker plot because for this one it is necessary to know/consider previously the multiplicity of secondaries.

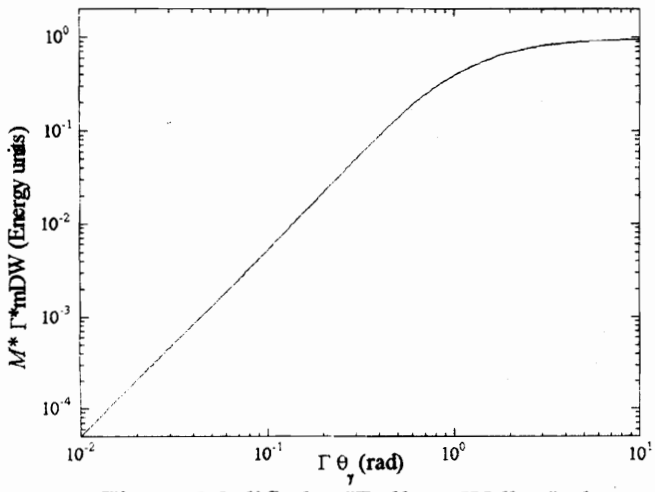

Fig. 1 - Modified - "Duller - Walker" plot

We re-analyzed C-jets of various experiments (Chamber 15, 16, 17, ...) in a total of 90 events. Extracting the isotropic events only,

$$R = (\Sigma E)(\Sigma E\theta^2) \Big/ \left[\frac{4}{\pi}\Sigma E\theta\right]^2$$

has a behavior like fig. 2. This is possible through a convenient combination of moments[3] .

Applying the algorithm mDW to these selected events we obtained fig. 3 where it is clear the separation in two regions, the left region occupied by the events called Mirim type and the right region by Açú type, since B-J Collaboration notation. After the separation of events we can do analysis to obtain characteristics of each type of fire-balls and our preliminary analysis yields results similar to the previous results obtained by B-J Collaboration.

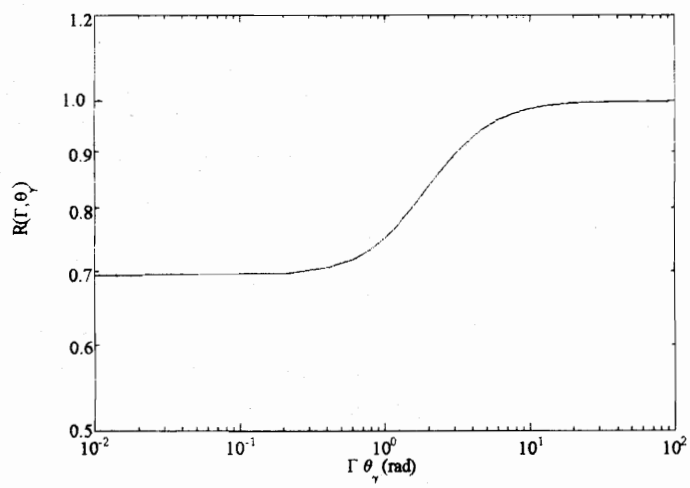

Fig. 2 - Moments ratio

Discussions and Conclusions

By the use of this modified Duller-Walker plot, we obtained a clear separation of events in two types, consistent with previous B-J Collaboration results. So, these results indicate occurrence of events obeying Feynman scaling and other set of events showing Feynman scaling law breaking.

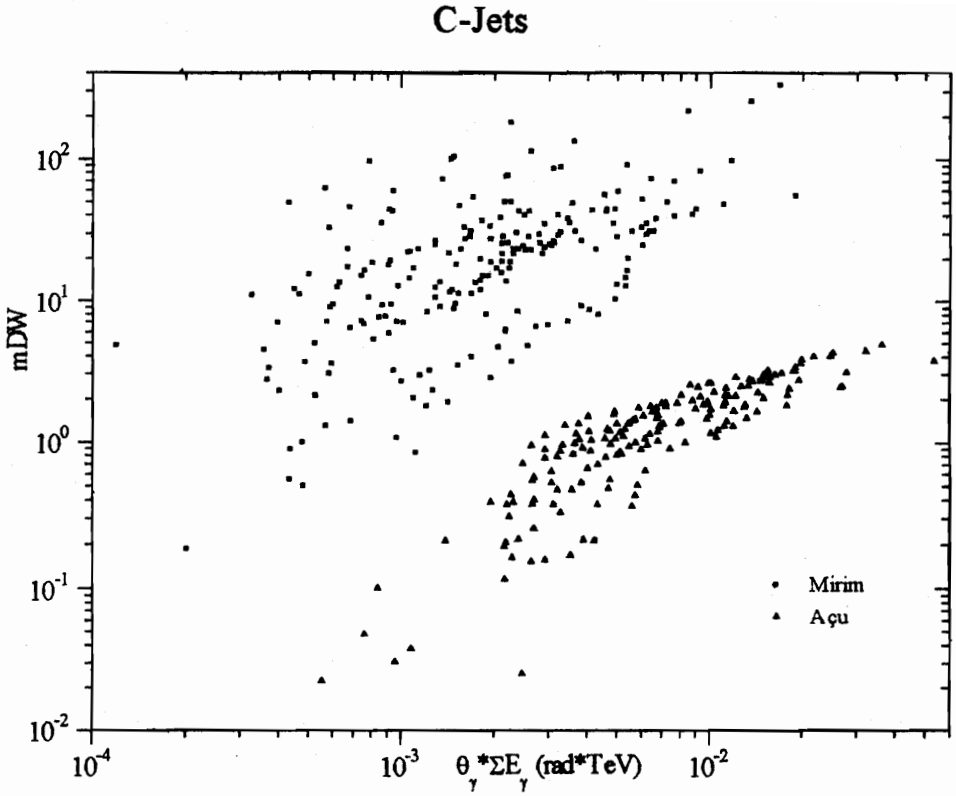

Fig. 3a - mDW applied to isotropic C-Jets

Acknowledgments

The authors are grateful to B-J Collaboration for the free use of the data. The experiments of B-J Collaboration are supported by FAPESP, CNPq, FINEP in Brasil, by Ministry of Education of Japan and are held in the Mt. Chacaltaya, La Paz-Bolivia with the collaboration of Instituto de Investigaciones Fisicas-UMSA.

References

[1] Duller N. and Walker W., Phys. Rev.93 (1954),215

[2] Chacaltaya Emulsion Chamber Experiment, Suppl. Prog.Theo.Phys.47(1971),1

[3] Shibuya EH, Proc. XVIII ICRC/IUPAP vol.11, Bangalore-India (1983),97.

A Double-core Event Detected at Chacaltaya

N.M.Amato[1], R.H.C.Maldonado[2] and H.M.Portella[2]
[1] Centro Brasileiro de Pesquisas Físicas, RJ, Brasil
[2] Instituto de Física - UFF, Niterói, RJ, Brasil

Abstract

We describe a cosmic-ray induced event, CH24 S23 I10, observed in the 24th chamber exposed by Brasil-Japan Collaboration. The event is of clear double-core type consisting of 2 groups, one with $\Sigma E_\gamma = 971.8$ TeV and the other with $\Sigma E_\gamma = 880.8$ TeV. The distance between the two energy weighted centers is 5.7 mm.

1 Introduction

Brasil-Japan Collaboration has been studying the cosmic ray interactions in the energy region $10^{13} - 10^{17}$ eV by means of emulsion chambers exposed at Chacaltaya (5220 m above sea-level), Bolivia [1]. In this paper are described the characteristics of a family of γ-rays (and hadrons) detected in the 24th chamber at Chacaltaya. The total measurable energy is $\Sigma E_\gamma = 3146.2$ TeV.

2 Experiment

The detector, in which our event was found consists of an upper chamber (4 cm of Pb), a target layer (30 cm of polyethylene), an air space (181 cm of air) and a lower chamber (6 cm of Pb). Both the upper chamber (42 m^2) and the lower chamber (13.6 m^2) are of multilayered sandwiches of lead plates and photosensitive materials. Each photosensitive layer consists of two sheets of X-ray films, and in a few of them, in the upper chamber, nuclear emulsions also are inserted. In the lower chamber only X-ray films are inserted. The showers were observed on X-ray films by naked eye scanning and then under microscope. The darkness of the spots on the X-ray films was measured with the microdensitometer, and energy of showers was determined according to the 3-dimensional EM cascade theory [2]. Many dark spots correspond to single showers, but a great number is produced by several showers that cannot be individualized, so that the darkness of these spots gives the total energy of the showers inside them.

3 Experimental Results

As the event was observed in the unit block 23 in the upper chamber and in the block 10 in the lower chamber, we name this event as CH24 S23 I10. Fig. 1

shows the photography of the event on the N-type X-ray film located at 10 c.u. in the upper chamber. The target diagram of the event is shown in Fig. 2, where we can see two separate groups of showers. One group has total observed energy $\Sigma E_\gamma = 971.8$ TeV, and the other has the energy $\Sigma E_\gamma = 880.8$ TeV. The distance between the energy weighted centers of the two groups is 5.7 mm. Outside the two groups there are many showers with $\Sigma E_\gamma = 1293.6$ TeV; so, for the total energy of the event results the value $\Sigma E_\gamma = 3146.2$ TeV. Some showers continue from the upper to the lower chamber. Unfortunately this continuation is located near the edge of the X-ray films, so that many showers may be lost and others are seen only in one layer.

Fig. 1 Photography of the event CH24 S23 I10

Fig. 2 Target diagram of the event CH24 S23 I10

Fig. 3 shows the integral energy spectrum of γ-rays; the straight line represents an exponential spectrum.

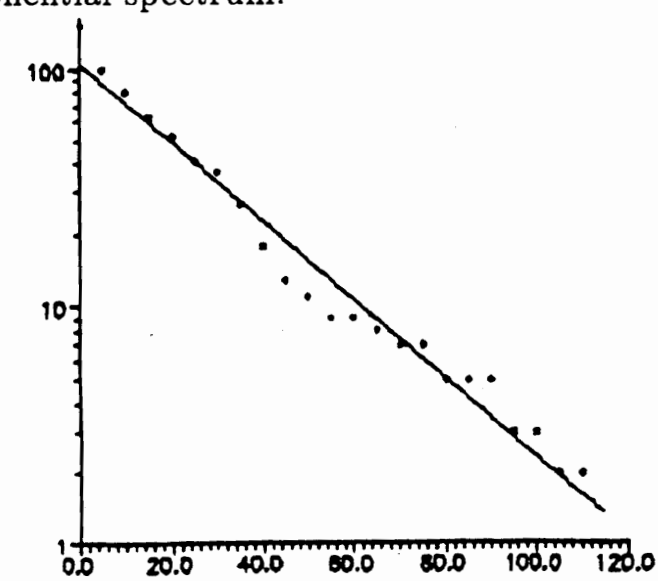

Fig. 3 Integral energy spectrum of γ-rays

As the event is composed of two groups, we present, in Table 1, the characteristics of each group separately.

TABLE 1

Group	ΣE_γ (TeV)	$< ER >$ (TeV mm)
1	971.8	25.14
2	880.8	22.10

The energy weighted spread of the whole event is $< ER >= 424$ TeV mm.

Acknowledgements

The authors wish to acknowledge all the members of the Brasil-Japan Collaboration for their kind support. Thanks are due to Prof. A.Osawa for valuable discussions; to T.T. Villar for the scanning and measurements, to the student A.M.M. de Lima for the computer calculation, to A.C. do Carmo for the photography. They also thank to CNPq, FAPESP for financial support to the Brazilian side of the Collaboration.

References

[1] Lattes C.M.G., Fujimoto Y. and Hasegawa S., Phys. Rep. **65**, n.3 (1980) 151.

[2] Ohta I., Suppl. Progr. Theor. Phys. **47** (1971) 271.

Analysis of the Particle Production in Cosmic Ray Events Detected at Chacaltaya

N.Amato[1], R.H.C.Maldonado[2] and H.M.Portella[2]
[1] Centro Brasileiro de Pesquisas Físicas, RJ, Brasil
[2] Instituto de Física - UFF, Niterói, RJ, Brasil

Abstract

We are analysing the high energy interactions detected in the 24th emulsion chamber exposed at Chacaltaya (5220 m).
The aim of this paper is to continue the investigation of the azimuthal effect on the transverse characteristics and the energy in the gamma hadron families to clear the dynamic mechanism of hadron nuclei collisions.

1 Introduction

The 24th two story nuclear emulsion chamber of Brasil-Japan Collaboration was exposed together with the air-shower array at Chacaltaya. The arrangement of this exposure is seen in the Fig. 1.

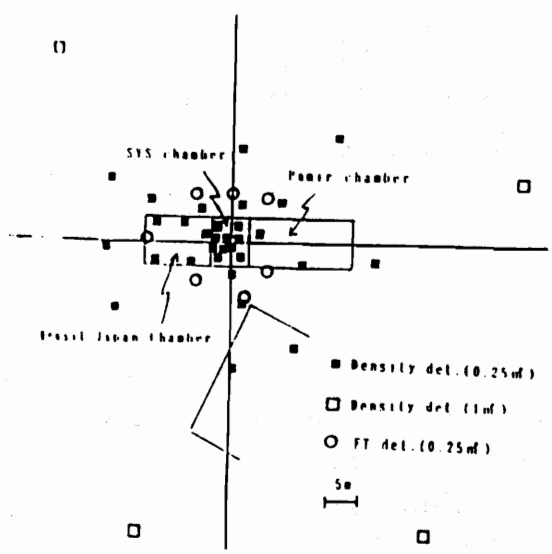

The families observed in this chamber can be linked with the accompanied air showers, when the air shower size is large, say, exceeding 10^7 [1]

In the photosensitive material analysed at CBPF, Rio de Janeiro (50 blocks, corresponding to an area of 10,0 m^2) we found 35 families with

$\Sigma E_\gamma > 30$ TeV, among which, 12 have $\Sigma E_\gamma > 100$ TeV including one consisting of two groups of showers, with total energy of $\Sigma E_\gamma > 3000$ TeV [2]. The correlation between the more energetic families and the air showers will be made in the future.

2 Results

We are investigating the dependence of the azimuthal effects on the spatial characteristics in these families.

We analysed the events with $\Sigma E_\gamma = 100 - 300$ TeV and, separately, the special event with $\Sigma E_\gamma > 3000$ TeV. To verify if the anisotropy effect appears in these events, we obtained the superposition of the eight first harmonics of Fourier analysis for each family.

Fig. 2 shows the result for the special event with two groups of showers.

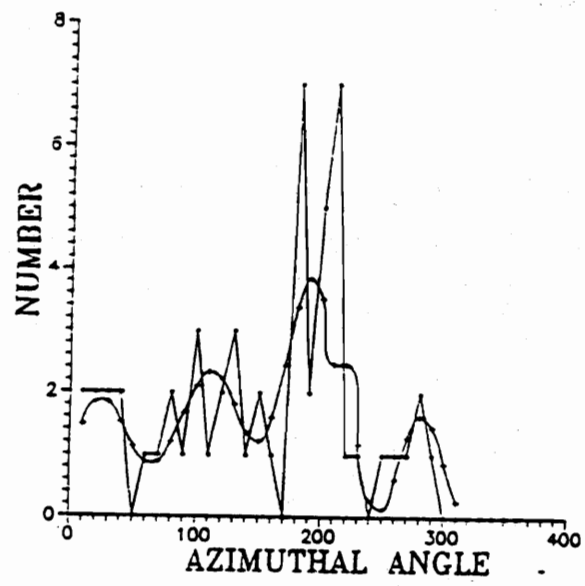

To investigate the azimuthal correlation we used a statistical criterion sensitive to the mechanism of nuclear interaction calculating the value of the α parameter [3] and the quantity λ [4].

We applied the "decascading" and "jet analysis" procedure using $k_{dec} =$ 12 TeV mm and $k_{jet} = 250$ TeV mm [5], respectively, for all families cited above.

The families were selected according to the criteria of $N_\gamma > 5$ and $E_{th} =$ 4 TeV. In the special event of $\Sigma E_\gamma > 3000$ TeV, we made calculations also for different values of E_{th}.

The results of these calculations are shown in the Tables 1 and 2.

TABLE 1

$\Sigma E_\gamma 100-300$ TeV				
Before Decascading		After Decascading		
$<\alpha>$	$<ER>$	$<\alpha'>$	$<E'R'>$	$<\lambda>$
0,19	183,6	0,08	277,09	0,16

TABLE 2

Event with $\Sigma E_\gamma > 3000$ TeV					
	Before Decascading		After Decascading		
E_{th}	α	$<ER>$	α'	$<ER'>$	$<\lambda>$
4 TeV	0,03	424,4	0,05	1235,6	0,18
10 TeV	0,02	1318,8	0,14	1748,1	0,15
15 TeV	0,15	1704,8	0,17	1698,9	0,15
50 TeV	0,37	2157,9	0,42	2164,2	0,23
100 TeV	0,94	3100,3	0,94	3113,4	0,31

We investigated if the parameter $<\alpha>$ depends strongly on the mean value of ER where R is measured from the center of the event.

As the results on particle accelerator experiments have showed that the production of jets of particles with big momenta increases with the energy, we investigated if this effect appears in these cosmic ray families.

We made a comparison between our events and those calculated taking into account the jets generation on the basis of QCD [6], and we observed that there is an agreement with the results obtained by Azimov et al [3].

We observed that the average number of jets produced increases with the total energy. We found $<N_{jet}>=2$ for the families with $\Sigma E_\gamma = 100-300$ TeV and $<N_{jet}>=6$ for the special event $\Sigma E_\gamma > 3000$ TeV.

Acknowledgements

The authors thanks the members of the Brasil-Japan Collaboration and also T.T. Villar and the student A.M.M. de Lima for their help.

References

[1] Kawasumi N. et al, Proceedings of VIII International Symposium on Very High Energy Cosmic Ray Interactions, Tokyo, Japan (1994) 253.

[2] Amato N. et al, Contributed paper to this conference, (1995).

[3] Azimov S.A. et al, 16th ICRC, Kyoto, Japan (1979) 262.

[4] Pamir Collaboration, 22nd ICRC, Dublin, Ireland, **4** (1991).

[5] Semba H., Progr. Theor. Phys., Supp. 76 (1983), 11.

[6] Gribov C.V., Levin E.M. and Ruskin M.G., Phys. Let. B, **121**, 7 (1983) 65.

Nucleon-Air Nuclei Interaction Probability Law and the Inelastic Cross-Section

H.M.Portella[1], N.Amato[2], R.H.C.Maldonado[1], A.Gomes[1] and C.E.C.Lima[2]
[1] Instituto de Física/UFF, Niterói, RJ - Brasil
[2] Centro Brasileiro de Pesquisas Físicas, RJ - Brasil

Abstract

We integrated exactly the Nucleon Diffusion Equation using the successive approximation method with the primary energy spectrum in the general form, $G(E)$.
We considered the nucleon-air nuclei inelastic cross-section rising with energy in three different forms (logarithmic, logarithmic square and power function). The Interaction Probability law for the first and second cases is binomial and for the third case is a hypergeometrical function. If the inelastic cross-section is constant this law is Poissonian.

1 Nucleon Diffusion Equation

This paper is a continuation of the previous results published in the Proceedings of Int. Symp. on Cosmic Ray Super High Energy Interactions (1988), Lodz-Poland [1].

Assuming, a priori, that the probability of a nucleon making n interactions in traversing a depth x of the atmosphere is given by the Poisson Distribution, G. Brooke et. al. [2] obtained for the total Intensity of Nucleons at x the following expression

$$F_N(x,E) = e^{-x/\lambda} \sum_{n=0}^{\infty} \left(\frac{x}{\lambda\eta}\right)^n \frac{1}{n!} G\left(\frac{E}{\eta^n}\right) \tag{1}$$

where $G(E)$ is the primary nucleon energy spectrum, λ is the interaction length, η is the elasticity coefficient, both supposed constants.

We used the successive approximation method to integrate exactly the differential equation that describes the diffusion of a nucleon in the atmosphere,

$$\frac{\partial F_N(x,E)}{\partial x} = -\frac{F_N(x,E)}{\lambda(E)} + \frac{F_N(x,E/\eta)}{\eta\lambda(E/\eta)} \tag{2}$$

with the boundary condition $F_N(0,E) = G(E)$ and $\lambda(E)$ is the nucleon-air nuclei interaction mean free path supposed a function of the energy.

The solution for $\lambda(E)$ in the general form is the following

$$F_N(x,E) = \sum_{n=0}^{\infty} e^{-x/\lambda(E_0\eta^n)} \varphi_n(x, \delta\,(E_0,\eta))\, \xi_n(E) G(E/\eta^n)\, \frac{1}{\eta^n} \tag{3}$$

where

$$\xi_n(E) = \frac{1}{\lambda(E/\eta)\lambda(E/\eta^2)\cdots\lambda(E/\eta^n)} \tag{4}$$

and $\varphi_n(x, \delta(E_0,\eta))$ represents the multiple integral calculated by induction, with the solution

$$\varphi_n(x, \delta(E_0,\eta)) = \frac{1}{n!}\left(\frac{1-e^{-\delta(E_0,\eta)x}}{\delta(E_0,\eta)}\right)^n \tag{5}$$

2 Results and Discussions

The total nucleon flux, $F_N(x,E)$, can be also expressed in the following way,

$$F_N(x,E) = \sum_{n=0}^{\infty} \frac{P_n(x,E_0)\, G(E_0)}{\eta^n} \tag{6}$$

where $P_n(x,E_0)$ is the probability that a nucleon with energy $E_0 = E/\eta^n$ at $x = 0$ interacts n times down to the depth x and it assumes different forms for different dependences of the interaction length with energy;

$$\lambda = \text{constant} \rightarrow \text{Poisson Distribution}$$

$$\lambda = \lambda_0 \left(\frac{E}{\varepsilon}\right)^{-a} \rightarrow P_n(x,E_0) =$$

$$= \frac{e^{-x/\lambda(E_0\eta^n)}\,(1-e^{-\delta(E_0,\eta)x})^n\,\eta^{-\frac{a}{2}(n+1)n}}{n!(\eta^{-a}-1)^n} \tag{7}$$

$$\lambda = \lambda_0 \left(1 + a\,\ln\left(\frac{E}{\varepsilon}\right)\right)^{-1} \rightarrow P_n(x,E_0) =$$

$$= \frac{e^{-x/\lambda(E_0\eta^n)}}{n!\Gamma(Z+1)}\,\Gamma(Z+1+n)(1-e^{-\delta(\eta)x})^n \tag{8}$$

with $Z = \frac{1+a\ \ln E/\varepsilon}{\delta(\eta)\lambda_0}$.

$$\lambda = \lambda_0 a\ \ln^{-2}\left(\frac{E}{\varepsilon}\right) \rightarrow P_n(x, E_0) =$$

$$= \frac{e^{-x/\lambda(E_0\eta^n)}(1 - e^{-\delta(E_0\eta)x})^n}{n!\,\frac{a}{\lambda_0}\,(1-2Y)^n}\left\{\frac{\Gamma(n+1-Y)}{\Gamma(1-Y)}\right\}^2 \tag{9}$$

with $Y = \frac{\ln E/\varepsilon}{\ln \eta}$.

In the case of constant cross-section, $P_n(E_0, x)$ is purely poissonian but for $\sigma = \sigma(E)$ the distributions are distorted to a large number of interactions. In these cases the differential equation (2) is not good to describe the diffusion of nucleons in the atmosphere.

It is important to note, that for the case of Poisson Distribution, the interaction of nucleon is independent of the depth x; in the other cases ($\sigma = \sigma(E)$) this fact is not verified.

Acknowledgement

The authors would express their thanks to professor F.M.O. Castro, in memorium, for valuable discussions.

References

[1] Portella H.M. and Castro F.M.O., Proc. of Int. Symp. on Cosmic Ray Super High Energy Interactions, Lodz/Poland (1988).

[2] Brooke G., et al., Phys. Soc. **83** (1966) 853.